

A new universal ratio in Random Matrix Theory and chaotic to integrable transition in Type-I and Type-II hybrid Sachdev-Ye-Kitaev models

Fadi Sun,^{1,2,3,4} Yu Yi-Xiang,^{5,6} Jinwu Ye,^{1,2,3,4} and W.-M. Liu⁵

¹*Institute for Theoretical Sciences, Westlake University, Hangzhou, 310024, Zhejiang, China*

²*Tsung-Dao Lee Institute, Shanghai 200240, China*

³*Department of Physics and Astronomy, Mississippi State University, MS 39762, USA*

⁴*Kavli Institute of Theoretical Physics, University of California, Santa Barbara, Santa Barbara, CA 93106, USA*

⁵*Beijing National Laboratory for Condensed Matter Physics, Institute of Physics, Chinese Academy of Sciences, Beijing 100190, China*

⁶*Beijing Institute of Science and Technology, Beijing 100083, China*

(Dated: December 21, 2021)

We investigate chaotic to integrable transition in two types of hybrid SYK models which contain both $q = 4$ SYK with interaction J and $q = 2$ SYK with an interaction K in type-I or $(q = 2)^2$ SYK with an interaction \sqrt{K} in type-II. These models include hybrid Majorana fermion, complex fermion and bosonic SYK. For the Majorana fermion case, we discuss both N even and N odd case. We make exact symmetry analysis on the possible symmetry class of both types of hybrid SYK in the 10 fold way by Random Matrix Theory (RMT) and also work out the degeneracy of each energy levels. We introduce a new universal ratio which is the ratio of the next nearest neighbour (NNN) energy level spacing to characterize the RMT. We perform exact diagonalization to evaluate both the known NN ratio and the new NNN ratio, then use both ratios to study Chaotic to Integrable transitions (CIT) in both types of hybrid SYK models. Some preliminary results on possible quantum analog of Kolmogorov-Arnold-Moser (KAM) theorem and its dual version in the quantum chaotic side are given. We explore some intrinsic connections between the two complementary approaches to quantum chaos: the RMT and the Lyapunov exponent by the $1/N$ expansion in the large N limit at a suitable temperature range. We stress the crucial differences between the quantum phase transition (QPT) characterized by renormalization groups at $N = \infty$, $1/N$ expansions at a finite N and the CIT characterized by the RMT at a finite N : the former focus on the ground state and its low energy excitations (edge states in the Fock space), the latter on excited states (bulk states in the Fock space). We also discuss Eigenstate Thermalization hypothesis (ETH)'s power on a quantum chaotic bulk state and its inability to encode the edge states. Comments on some previously related works are given. Some future perspectives, especially the failure of the Zamolodchikov's c -theorem in 1d CFT RG flow are outlined.

I. INTRODUCTION

In classical chaos, the Lyapunov exponent was used to characterize the exponential growth of two classical trajectories when there are just a tiny difference in the initial conditions. The classical concept of Lyapunov exponent can be extended to its quantum analog to characterize the exponential growth of two initially commuting operators in the early time (up to the Ehrenfest time) under the evolution of a quantum chaotic Hamiltonian¹⁻³. There are recent flurry of research activities to extract the Lyapunov exponent λ_L of the Sachdev-Ye-Kitaev (SYK) model and its various variants through evaluating out of time ordered correlation (OTOC) functions⁴⁻¹⁵. The quantum analog of λ_L need to be evaluated away from the thermodynamic limit by a $1/N$ expansion in the SYK models, also away from the conformal invariant limit due to a leading irrelevant operator and at a finite temperature (ranging from low to infinite temperatures). There are also calculations in the dual bulk quantum black holes in an asymptotic AdS_2 geometry to demonstrate the correspondence between the SYK models and Jackiw-Teitelboim gravity¹⁶⁻¹⁹. The quantum chaos in the SYK models are due to the quenched disorders and interac-

tions. However, it inspired a new class of clean models called (colored or un-colored) Tensor (Gurau-Witten) model³⁰⁻³², which share similar quantum chaotic properties as the SYK models at least in the large N limit.

From a completely different perspective and also at a much longer time scale (Heisenberg time), the quantum chaos can also be characterized by the system's energy level-level correlations encoded in the energy level statistics (ELS) and the spectral form factor (SFF) through random matrix theory (RMT)²⁰⁻²². The ELS and SFF are always evaluated in a finite but sufficiently large system²³⁻²⁷. The ELS of SYK can be described by the Wigner-Dyson (WD) distributions in a $N \pmod{8}$ way^{23-25,29}: $N = 2, 6$ Gaussian unitary ensembles (GUE), $N = 0$ Gaussian orthogonal ensemble (GOE), $N = 4$ Gaussian symplectic ensemble (GSE).

Here we investigate chaotic to integrable transitions (CIT) in two types of hybrid SYK models. The type-I contains both the chaotic $q = 4$ SYK with interaction J and the integrable $q = 2$ SYK with interaction K . It violates the particle-hole (PH) symmetry and includes the hybrid Majorana fermion, complex fermion and hard-core bosonic SYK. The type-II includes $q = 4$ SYK of either Majorana or complex fermion with interaction J and

$(q = 2)^2$ SYK with the interaction \sqrt{K} . It preserves the particle-hole (PH) symmetry. In this work, we mainly use the RMT approach, but will also explore some possible connections between the RMT approach and the Lyapunov exponent which can be extracted from the out of time correlation functions (OTOC).

There are direct motivations to study both types of Hybrid SYK models. It was also known that the $q = 4$ SYK model provides a concrete model to realize Eigen-state Thermalization Hypothesis (ETH)⁴³. Even the entanglement entropy of its ground state satisfies the volume law instead of the more common area law. Here it is important to study how the gapless quantum spin liquid (QSL) responses under the Type I or Type II kinds of integrable perturbations. It would also be interesting to study how the ETH breaks down under the Type I or Type II kind of integrable perturbations. On the dual bulk gravity side, these kind of perturbations are also needed to probe the interior behind the black hole horizon⁴⁵. Most importantly, in any possible experimental systems to realize SYK models, the Type I and Type II terms are most common perturbations. As shown in Fig.9 in the conclusion section, the two types hybrid SYK models also provide specific examples of RG flow between two CFT_1 fixed points which violate Zamolodchikov's c-theorem. When comparing with some previously studied hybrid models, one can see there are also many other motivations to study both types of hybrid SYK models. For example, the multi-channel Kondo models show non-Fermi liquid (NFL) behaviours, so it is important to study how the NFL changes under spin or channel anisotropy^{36,38-40}. The Kitaev honeycomb lattice model⁴¹ hosts a Majorana fermion quantum spin liquid (QSL), so it is important to study how the Majorana fermion QSL changes under adding other interactions such as a Heisenberg interaction or a Dzyaloshinskii-Moriya (DM) term⁴².

We first introduce a new universal ratio which is the ratio of next nearest neighbor (NNN) energy spacing to characterize the RMT classes and also establish its relations with the well-known ratio of the nearest neighbor (NN) energy spacing⁴⁶. When a doubly degenerate level is split by a small perturbation, the NN ratio is nearly zero and also rapidly changing, the new NNN ratio can be used to effectively characterize the "hidden" RMT behaviours, especially the CIT. We make exact symmetry analysis to classify the possible symmetry class in the 10-fold way^{29,47,50}, and then perform exact diagonalization (ED) on all these hybrid models. In the Majorana fermion case, we pay special efforts to classify the odd N case. Both the NN ratio and the NNN ratio are evaluated when a doubly degenerate level is split by a small perturbation. In the type-I hybrid SYK, as K/J increases, there is always a chaotic to integrable transition (CIT) from GUE to Poisson in all the hybrid Majorana or complex fermionic models, but not the hybrid bosonic model. Starting from the type-I hybrid $q = 4$ Majorana or complex fermion SYK side, for the GOE case, there is a GOE to GUE crossover first, then a CIT from the GUE to the

Poisson; for the GUE case, there is a direct CIT from the GUE to the Poisson; for the GSE case, any small K destroys the double degeneracy of the GSE, the NN ratio rises to GUE, then a CIT from the GUE to the Poisson. In this case, the NNN ratio can be most effectively applied to describe the stability regime of GSE near the chaotic side and may also be used to describe the whole crossover until to the integrable side.

In the type-II hybrid SYK, the symmetry analysis alone may not be able to distinguish between the chaotic $q = 4$ SYK and integrable $(q = 2)^2$ SYK. As K/J increases, there are always CIT from the corresponding WD distribution dictated by the symmetry of the $q = 4$ SYK to the Poisson controlled by the $(q = 2)^2$ SYK. When there is a double degeneracy at the $(q = 2)^2$ side, the NNN can be most effectively applied to describe the CIT and may also be used to describe the whole crossover until to the quantum chaotic side.

In classical chaos, the classical Kolmogorov-Arnold-Moser (KAM) theorem states that if an integrable Hamiltonian H_0 is disturbed by a small perturbation ΔH , which makes the total Hamiltonian $H = H_0 + \Delta H$ non-integrable. If the two conditions are satisfied: (a) ΔH is sufficiently small (b) the frequencies ω_i of H_0 are incommensurate, then the system remains quasi-integrable. Despite some previous efforts, the quantum analogue of the KAM theorem remains elusive. Just like the quantum analog of Lyapunov exponent can be studied in the context of the SYK models⁴⁻¹⁶, it is important to explore the quantum analog of KAM theorem in both types of hybrid SYK models. We first give a definition of the quantum analogue of the KAM theorem and also its possible dual form which is the stability of quantum chaos in the context of RMT. Then we use both NN and NNN ratio to numerically characterize the KAM regime in the integrable side and the stability of quantum chaos in the chaotic side. We give some preliminary results on possible quantum analog of the KAM theorem, the stability of quantum chaos (can also be called the dual form of the KAM theorem), especially its dependence on the system's size N in the two types hybrid SYK models. By pushing the methods developed in⁷⁰ further, we leave rigorous mathematical treatments to a future publication⁷¹.

We also stress the crucial differences between the onset of quantum phase transitions (QPT) at $N = \infty$ characterized by renormalization group (RG), $1/N$ expansions and the onset of CIT characterized by the RMT at a finite N . The former is focusing on the changes in the ground state and low energy excitations (called edge excitations in the Fock space), there is an associated divergent length scale and quantum critical scalings and a finite size scaling at a finite size. While the latter is focusing on the changes in the correlations in the bulk energy levels in the Fock space, there is no associated divergent length scale, therefore no quantum critical scalings and no finite size scaling at a finite size. We also discuss Eigenstate Thermalization hypothesis (ETH)'s power on a quantum chaotic bulk state and its inability to encode

the ground state and low energy excitations. Some comments on previous works on type-I hybrid SYK models are given. Some perspectives and possible future directions are outlined in the conclusion section. Especially, we point out that the Zamolodchikov's c-theorem of 2d CFT and its extensions to 2d boundary CFT and higher dimensions break down in 1d CFT RG flow. This fact maybe related to $NAdS_2/NCFT_1$ may also be dramatically different than its high dimensional counterparts.

As mentioned in the first two paragraphs, there are two complementary approaches to describe the quantum chaos: the OTOC at an early time and the RMT at a later time. However, so far, it seems there is no clear connections between the two different ways to characterize the quantum chaos. In this work, we establish some intrinsic connections between the two approaches: the quantum chaos in the bulk energy levels described by the RMT implies the quantum information scramblings with a non-vanishing Lyapunov exponent λ_L by the OTOC in the edge levels (the ground state and low energy levels) in a suitable temperature range.

II. A NEW RATIO TO DESCRIBE RMT: RATIO OF NEXT NEAREST NEIGHBOR ENERGY SPACING

In this section, we first review the known results on the statistics of the NN energy level spacing (r, \tilde{r}), then introduce a new ratio which is the NNN energy level spacing (r', \tilde{r}'), then establish an approximate, but quite accurate relation between the two.

A. Review on the ELS of NN energy level spacings

Let $\{E_n\}$ be an ordered set of energy levels and $s_n = E_{n+1} - E_n$ are the NN spacings. By considering a 2×2 matrices system, Wigner derived a simple approximate expression for the distribution function $P(s)$ of the NN spacing,

$$P_{w,\beta}(s) = a_\beta s^\beta e^{-b_\beta s^2} \quad (1)$$

where $\beta = 1, 2, 4$ is the Dyson index for GOE, GUE and GSE respectively. It is also known that independent random energy levels would yield a Poisson distribution

$$P_p(s) = e^{-s} \quad (2)$$

However, in order to compare different results from different systems, the energy levels will need an unfolding procedure, which is not convenient when large enough statistics is not available. To get rid of the dependence on the local density of states, it is convenient to look at the distribution of the ratio of two adjacent energy level spacings^{23,46} $r_n = s_n/s_{n+1}$ which distributes around 1. This quantity has the advantage that it requires no unfolding since ratios of consecutive level spacings are independent of the local density of states.

By considering 3×3 matrices system, the authors in⁴⁶ obtained the Wigner-like surmises of the ratio of consecutive level spacings distribution

$$P_p(r) = \frac{1}{(1+r)^2}, \quad P_w(r) = \frac{1}{Z_\beta} \frac{(r+r^2)^\beta}{(1+r+r^2)^{1+3\beta/2}} \quad (3)$$

where $\beta = 1, 2, 4$ and $Z_\beta = 8/27, 4\pi/81\sqrt{3}, 4\pi/729\sqrt{3}$ for GOE, GUE and GSE respectively. The distribution $P_W(r)$ has the same level repulsion at small r as $P_W(s)$, namely, $P_W(r) \sim r^\beta$. However, the large r asymptotic behavior $P_W(r) \sim r^{-(2+\beta)}$ is dramatically different than the fast exponential decay of $P_W(s)$.

One may also compute the distribution of the logarithmic ratio^{23,46} $P(\ln r) = P(r)r$. Because $P(\ln r) dr$ is symmetric under $r \leftrightarrow 1/r$, one may confine $0 < r < 1$ and double the probability density $P(\tilde{r}) = 2P(r)$. Therefore, the above two distributions have two different sets of expected values of $\tilde{r} = \min\{r, 1/r\}$:

$$\begin{aligned} \langle \tilde{r} \rangle_p &= \int_0^1 2rP_p(r)dr = 2\ln 2 - 1 \approx 0.38629, \\ \langle \tilde{r} \rangle_w &= \int_0^1 2rP_{w,\beta=1,2,4}(r)dr \end{aligned} \quad (4)$$

which is $4 - 2\sqrt{3} \approx 0.53590$, $2\sqrt{3}/\pi - 1/2 \approx 0.60266$, $32\sqrt{3}/(15\pi) - 1/2 \approx 0.67617$ for GOE, GUE and GSE respectively.

B. Introduction and calculation of the ELS of NNN energy level spacings

When there are nearly double degenerated energy levels, we find that it is convenient to introduce next nearest-neighbor (NNN) spacings $s'_n = E_{2n+1} - E_{2n-1}$ and ratios $r'_n = s'_n/s'_{n-1}$. Here we study the distribution of the ratio of the two NNN spacings by exploring the exact calculation for 5×5 matrices.

For a Poisson ensemble, it is more convenient to work with $P(s_1, s_2, s_3, s_4)$ and the ratio of consecutive NNN level spacings is $r' = (s_3 + s_4)/(s_1 + s_2)$. The NNN ratio distribution can be calculated from

$$P_p^{(2)}(r') = \int \prod_{i=1}^4 ds_i P(s_1, s_2, s_3, s_4) \delta\left(r' - \frac{s_3 + s_4}{s_1 + s_2}\right). \quad (5)$$

Since energy levels are not correlated in Poisson ensemble, one can rewrite $P(s_1, s_2, s_3, s_4) = \prod_{i=1}^4 P_P(s_i)$ and evaluate the integral to obtain a simple result

$$P_p^{(2)}(r') = \frac{6r'}{(1+r')^4}. \quad (6)$$

It is easy to see that $P_p^{(2)}(r') \sim r'$ when r' is small, and $P_p^{(2)}(r') \sim r'^{-3}$ when r' is large. Interestingly, there is a NNN level repulsion in Poisson ensemble which intuitively can be understood due to the interruption of the intermediate level.

For various Gaussian ensembles, it is good to start from the joint probability distribution $\rho(E_1, E_2, E_3, E_4, E_5)$ and the ratio of consecutive NNN level spacings is $r' = (E_5 - E_3)/(E_3 - E_1)$. The NNN ratio distribution can be calculated from

$$P_{w,\beta}^{(2)}(r') = \int \prod_{i=1}^5 dE_i \rho(E_1, E_2, E_3, E_4, E_5) \delta\left(r' - \frac{E_5 - E_3}{E_3 - E_1}\right) \quad (7)$$

where the joint probability distribution takes the form

$$\rho(E_1, E_2, E_3, E_4, E_5) = C_\beta \prod_{1 \leq i < j \leq 5} |E_i - E_j|^\beta \prod_{i=1}^5 e^{-E_i^2/2}.$$

The integral can be simplified as

$$P_{w,\beta}^{(2)}(r') \sim \int_0^\infty dx \int_0^{rx} dy \int_0^x dz f(x, y, z, r'), \quad (8)$$

$$f(x, y, z, r') = e^{-\frac{1}{2}((2+2r'^2+r)x^2 + 2z^2 + 2y^2 + yz + (1-r')x(y-z))}$$

$$\times x[r'(1+r')x^3(r'x-y)(r'x+z)y(x+y)(x-z)z(y+z)]^\beta,$$

where \sim means the normalization constant is ignored. The integrals can be evaluated analytically, but its expression is lengthy. Here, we just show analytically its asymptotic behaviour: $P_{w,\beta}^{(2)}(r') \sim r'^{3\beta+1}$ when r' is small, and $P_{w,\beta}^{(2)}(r') \sim r'^{-3(\beta+1)}$ when r' is large. If comparing them with those of $P_W(r)$, one can see that the asymptotic behaviours of the NNN level statistics with index β are the same as those of the NN with index $3\beta + 1$ (See Eq.(10) below for all the ranges). Similar to the Poisson case discussed above, the intermediate energy level induces much stronger level repulsions between NNN. In Fig.1, we compare $P_{w,\beta}^{(2)}$ obtained from Eq.(8) against the numerical simulations of the corresponding WD ensembles. We find nearly perfect agreement in all ranges of r' .

It is easy to check that $P^{(2)}(r')$ have the same symmetry as $P(r)$, namely, $P^{(2)}(r') = \frac{1}{r'^2} P^{(2)}(\frac{1}{r'})$, thus we can still define a \tilde{r}' . From the NNN ratio distribution given in Eq.(6) for Poisson and Eq.(8) for WD, one can calculate expectation value for r' and \tilde{r}' as

$$\langle r' \rangle = \int_0^\infty dr' r' P(r'), \quad \langle \tilde{r}' \rangle = \int_0^1 dr' 2r' P(r') \quad (9)$$

which are listed in Table I.

C. An approximate but accurate relation between the ELS of NNN and those of NN

In fact, instead of lengthy results from exact evaluation of integral, we find an approximate relation between $P^{(2)}(r')$ and $P(r)$:

$$P_{w,\beta}^{(2)}(r) \approx P_{w,3\beta+1}(r) \quad (10)$$

The difference of the two was shown in Fig.2. The very small deviation shows that the approximation in

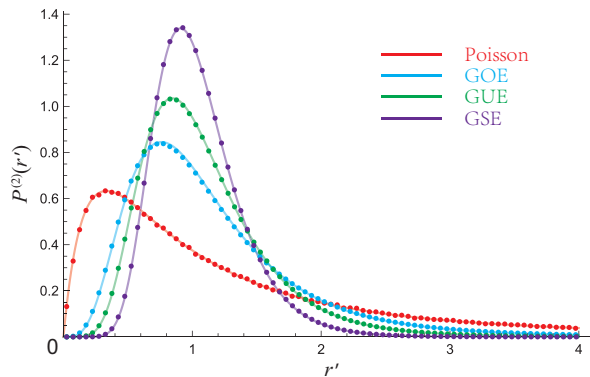


FIG. 1: Distribution of the ratio of consecutive NNN level spacings $P^{(2)}(r')$ for Poisson and RMT ensembles: solid lines are from exact evaluation of integral Eq.(8). The points are numerical data. The Poisson data are obtained from 10^6 independent generated random numbers. The random matrix data are obtained by diagonalizing the corresponding GOE (real), GUE (complex) and GSE (quaternion) matrices of size $N = 1000$ with Gaussian distributed entries, averaged over 10^5 histograms.

TABLE I: List of numerical values of averages $\langle r \rangle$ and $\langle \tilde{r} \rangle$ as well as $\langle r' \rangle$ and $\langle \tilde{r}' \rangle$ for various ensembles. The values of $\langle r \rangle$ and $\langle \tilde{r} \rangle$ are taken from Ref.⁴⁶. Those of $\langle r' \rangle$ and $\langle \tilde{r}' \rangle$ are obtained from evaluation of Eq.(9). We also list the values of $\langle r' \rangle_{3\beta+1}$ and $\langle \tilde{r}' \rangle_{3\beta+1}$ by using the $\beta \rightarrow 3\beta + 1$ rule in Eq.(10).

Ensembles	Poisson	GOE	GUE	GSE
$\langle r \rangle$	∞	1.75	1.3607	1.1747
$\langle \tilde{r} \rangle$	0.38629	0.5359	0.6027	0.6762
$\langle r' \rangle$	2	1.1736	1.0972	1.0516
$\langle \tilde{r}' \rangle$	0.5	0.6769	0.7344	0.7910
$\langle r' \rangle_{3\beta+1}$	–	1.1747	1.0980	1.0681
$\langle \tilde{r}' \rangle_{3\beta+1}$	–	0.6762	0.7335	0.7672

Eq.(10) is quite accurate. In the last two lines in the TABLE I, we also list the numerical values of $\langle r' \rangle_{3\beta+1}$ and $\langle \tilde{r}' \rangle_{3\beta+1}$ using $P_{W,3\beta+1}(r)$. All these values are very close to those using $P_{W,\beta}^{(2)}(r)$ in Eq.8. For example, just take $\langle \tilde{r}' \rangle$ for the GSE case, one can see the relative difference $\frac{0.7672 - 0.7910}{0.7910} = -3\%$ is very small.

In fact, one can see Eq.10 can also work well when putting $\beta = 0$. Namely, when the NN satisfies Poisson, the NNN seems fit GOE approximately. For example, from the TABLE I, $\langle r' \rangle$ and $\langle \tilde{r}' \rangle$ for Poisson are 2 and 0.5 which are not too much away from $\langle r \rangle$ and $\langle \tilde{r} \rangle$ for GOE (1.75 and 0.53590). At least, one can use GOE for an quick eye guides to judge the NNN for the Poisson as we did in all the following figures.

In the following sections, we will apply both NN and NNN ELS to study the CIT in the two types of hybrid Sachdev-Ye-Kitaev models.

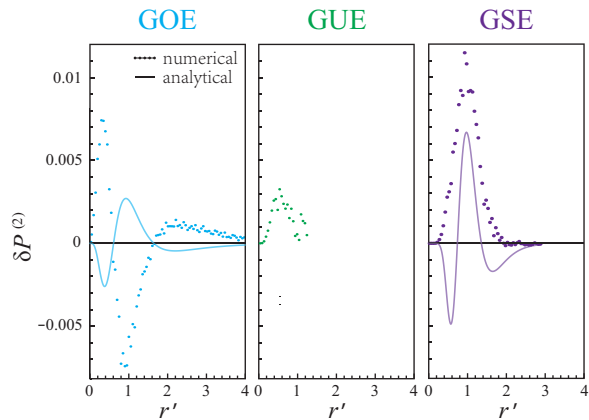


FIG. 2: Difference of $\delta P^{(2)} = P_{W,\beta}^{(2)}(r) - P_{W,3\beta+1}(r)$. The solid line is from Eq.8. The numerical data in $\delta P^{(2)} = P_{\text{num}}^{(2)}(r) - P_{W,3\beta+1}(r)$ are taken from Fig.1. Small $|\delta P^{(2)}|$ justifies validation of Eq.(10)

III. TYPE-I HYBRID SACHDEV-YE-KITAEV MODELS

By Type-I, we mean the integrable side is given by $q = 2$ SYK which breaks the PH symmetry Eq.12 of the $q = 4$ SYK. We will discuss Majorana and complex type-I hybrid SYK respectively.

A. The hybrid of $q = 2$ and $q = 4$ Majorana fermion SYK

The CIT may be first investigated in the hybrid of $q = 2$ and $q = 4$ Majorana fermion SYK, which also known as type-I hybrid Majorana SYK model:

$$H_{M-1} = \sum_{i < j < k < l}^N J_{ijkl} \chi_i \chi_j \chi_k \chi_l + i \sum_{i < j}^N K_{ij} \chi_i \chi_j \quad (11)$$

where J_{ijkl}, K_{ij} are real and satisfy the Gaussian distributions with $\langle J_{ijkl} \rangle = 0, \langle J_{ijkl}^2 \rangle = 3!J^2/N^3$ and $\langle K_{ij} \rangle = 0, \langle K_{ij}^2 \rangle = K^2/N$ respectively. In the following, we denote the first term of H_{M-1} , $q = 4$ SYK model, as H_{M4} , and the second term, $q = 2$ SYK model, as H_{M2} .

In the $J = 0$ limit, the $q = 2$ SYK H_{M2} breaks the PH symmetry Eq.12. It is non-interacting, so must be integrable. Its single particle density of state (DOS) satisfies the semi-circle law¹¹, while its many body ELS satisfies the Poisson distribution^{9,11,25}. Its many body low or high energy excitation level spacing is $\sim 1/N$, the low energy quasi-particle picture holds. Its $T = 0$ entropy density s_0 vanishes. This is very similar to the $U(1)/Z_2$ Dicke model⁶⁴⁻⁶⁸ in the $U(1)$ limit (inside the superradiant phase) where the many body ELS also satisfies the Poisson distribution, and the low energy excitation level spacing is also $\sim D \sim 1/N$ where D is the phase diffusion constant.

In the $K = 0$ limit, the $q = 4$ SYK Hamiltonian H_{M4} is non-integrable at any finite N . In the following, we discuss when N is even or odd respectively. For even number of sites $N = 2N_c$, one can split the sites to even and odd, then introduce N_c complex fermions^{10,23,25} by $c_i = (\chi_{2i} - i\chi_{2i-1})/\sqrt{2}, c_i^\dagger = (\chi_{2i} + i\chi_{2i-1})/\sqrt{2}$ and define the PH symmetry operator to be⁵²

$$P = K \prod_{i=1}^{N_c} (c_i^\dagger + c_i) \quad (12)$$

It is easy to show $P^2 = (-1)^{\lfloor \frac{N_c}{2} \rfloor}, P c_i P = \eta c_i^\dagger, P c_i^\dagger P = \eta c_i, P \chi_i P = \eta \chi_i$ where $\eta = (-1)^{\lfloor \frac{N_c-1}{2} \rfloor}$. The total number of fermions $Q_c = \sum_{i=1}^{N_c} c_i^\dagger c_i$. It is not a conserved quantity, but the parity $(-1)^{Q_c}$ is in H_{M4} . Then $P Q_c P^{-1} = N_c - Q_c$ which justifies P as an anti-unitary PH transformation. P also commutes with the Hamiltonian⁵¹ $[P, H_{M4}] = 0$. Depending on $N \pmod{8}$, the ELS satisfies GUE when $N \pmod{8} = 2, 6$, GOE when $N \pmod{8} = 0$, GSE when $N \pmod{8} = 4$ ^{10,23,25}. The ELS, the degeneracy at a given parity sector, and the total parity sector are listed in the Table IIa. Its low or high energy excitation level spacing is $e^{-s_0 N}$ which leads to extensive $T = 0$ entropy $s_0 = 0.232424\dots$ (in the $N \rightarrow \infty$ limit before $T \rightarrow 0$ limit)^{5,7,9}. The system's many body DOS (different from the single particle DOS) has been worked out in⁹ to be similar, but different than the semi-circle DOS. The quasi-particle picture completely breaks down. This is similar to the $U(1)/Z_2$ Dicke model in the Z_2 limit (inside the superradiant phase) where the ELS satisfies the GOE distribution^{67,68} (See Sec V-C), its two lowest energy splitting between two opposite parities is e^{-N} which is due to the instanton quantum tunneling (QT) process. Of course, the ground state of $q = 4$ SYK is a gapless quantum spin liquid. While that of $U(1)/Z_2$ Dicke model is a gapped Z_2 symmetry broken super-radiant state at $N = \infty$.

However, when N is odd, the above procedures for even N needs to be modified. In fact, one can still take the advantage of the above representation with N even case by adding $\chi_{N+1} = \chi_\infty$ to make the parity conservation explicitly, but also enlarge the Hilbert space twice. Similar strategy was used before to study the symmetry protected topological phase of odd number of Majorana chain⁵⁶ and the ELS of the SYK model with N odd^{23,53}. Then one can still define P with $N_c = \frac{N+1}{2}$ as before. All the commutation relations still apply.

So when $N \pmod{8} = 3, 7$, N_c is even, then $P^2 = -1, +1$ respectively. Under P , Q_c maps to the same parity sector. So it is in GSE and GOE with degeneracy $d = 2$ and $d = 1$ respectively at a given parity sector. When using the Z operator (see Eq.(13) below) which maps Q_c to $Q_c + 1$, so it establishes the connection between the two parity sectors. So it has the degeneracy $d_t = 2 + 2$ and $d_t = 1 + 1$ when considering both parities.

When $N \pmod{8} = 1, 5$, N_c is odd, then $P^2 = +1, -1$ respectively. However, under P , Q_c maps to the opposite

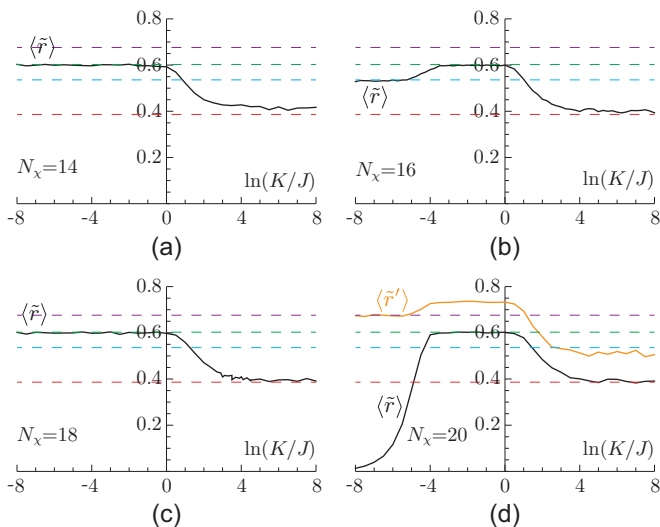


FIG. 3: Even N : the evolution of the ELS for type-I hybrid Majorana SYK model with even N . (a) and (c) are GUE, (b) is GOE, (d) is GSE on the $q = 4$ side. $\langle \tilde{r} \rangle$ (black curve), and $\langle \tilde{r}' \rangle$ (orange curve) for the GSE case in (d) evaluated for $N_x = 14, 16, 18, 20$ and are averaged over 100, 80, 60, 40 samplings respectively. Notably, in the GSE case in (d), the NN ratio $\langle \tilde{r} \rangle$ is rapidly changing near the $q = 4$ side, so it is quite difficult to determine the stability regime of the quantum chaos. Fortunately, the NNN ratio $\langle \tilde{r}' \rangle$ shows a nice plateau regime near the $q = 4$ side, the quantum chaos stability regime can be easily identified and listed in the Table III-VI. This dramatic advantage of the new NNN ratio over the known NN ratio when there is a double degeneracy was further demonstrated in all the following relevant figures when there are double degeneracy on the chaotic side or integrable side.

sector $Q_c + 1$. So one may only use P to establish the connection between the two opposite parity sectors. This forced us to look for a new operator which may map Q_c into the same sector and still commutes with the Hamiltonian. This new operator is found to be:

$$Z = P\chi_\infty = K \prod_{i=1}^{N_c-1} (c_i^\dagger + c_i) \quad (13)$$

which can be written down by just changing N_c in P to $N_c - 1$. So it will play a complementary role as P which will be analyzed in the following.

One can show that $Z\chi_i Z = (-1)^{N_c} \eta \chi_i$ where $i = \infty$ is excluded and the number $\eta = (-1)^{\lfloor \frac{N_c-1}{2} \rfloor}$ is defined below Eq.12. It is also easy to see that $Z^2 = \eta$. Using the fact that the Hamiltonian does not contain the fermions added at infinity, one can show that it still commutes with the Hamiltonian $[Z, H_{M4}] = 0$. It also leads to $ZQ_c Z^{-1} = N_c - 1 - Q_c + 2n_\infty$ where $n_\infty = c_\infty^\dagger c_\infty = \frac{1}{2} - i\chi_\infty \chi_N$.

So when $N \pmod{8} = 1, 5$, N_c is odd. Under Z , Q_c maps to the same sector. $Z^2 = 1$ and $Z^2 = -1$ respectively, so it is in GOE and GSE with degeneracy $d = 1$ and $d = 2$ respectively at a given parity sector.

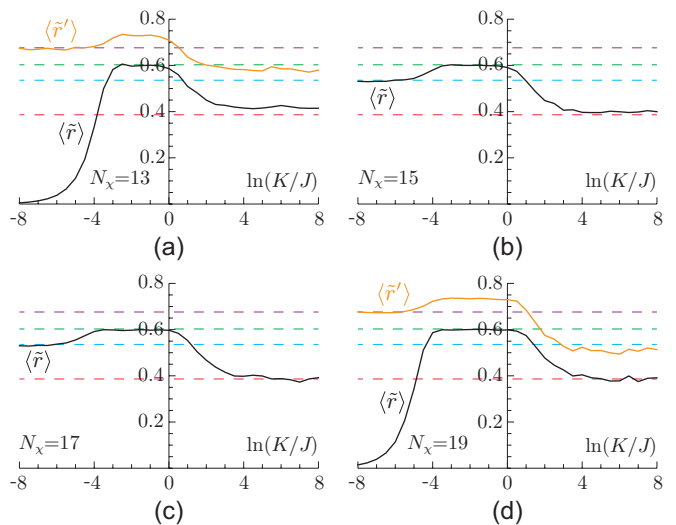


FIG. 4: Odd N : the evolution of the ELS for type-I hybrid Majorana SYK Model with odd N . (b) and (c) are GOE, (a) and (d) are GSE on the $q = 4$ side. $\langle \tilde{r} \rangle$ (black curve), and $\langle \tilde{r}' \rangle$ (orange curve) for the GSE case in (a) and (d) evaluated for $N_x = 13, 15, 17, 19$ and are averaged over 100, 80, 60, 40 samplings respectively. Note the advantages of using $\langle \tilde{r}' \rangle$ over $\langle \tilde{r} \rangle$, especially in the quantum chaos side, in (a) and (d).

When using the P operator (see above) which maps Q_c to $Q_c + 1$, so it establishes the connection between the two parity sectors. Then it has the degeneracy $d_t = 1 + 1$ and $d_t = 2 + 2$ when considering both parities.

Now we apply the PH transformation to the hybrid SYK model Eq.11. The parity $(-1)^{Q_c}$ remains to be conserved. However, P (when $N \pmod{8} = 1, 5$, one use Z , in all the other cases, one use P) is not conserved anymore due to $\{P, H_2\} = 0$ (or $\{Z, H_2\} = 0$). So the hybrid SYK does not have the PH symmetry anymore. Just from symmetry point of view (the 10-fold way classification scheme), the hybrid Majorana SYK Eq.11 belongs to the class A, so may satisfy GUE for any ratio of K/J . Our ED studies⁵⁷ at a given parity $(-1)^{Q_c}$ sector were shown in Fig.3 for even N and 4 for odd N . In the following, we will discuss them respectively.

For even N , there are 3 cases: (a) For $N \pmod{8} = 0$, the $q = 4$ Majorana fermion SYK at $K = 0$ is in GOE, the hybrid is in the GUE around $K/J = e^{-3.5} \sim 0.03$ to 1, there is a crossover from GOE to GUE first, then a CIT from GUE to the Poisson as K/J increases.

(b) For $N \pmod{8} = 2, 6$, the $q = 4$ Majorana fermion SYK at $K = 0$ is in GUE, it stays in the GUE until $K/J = 1$, then there is a CIT from GUE to the Poisson as K/J increases.

(c) For $N \pmod{8} = 4$, the $q = 4$ Majorana fermion SYK at $K = 0$ is in GSE at $K = 0$. Because $P^2 = -1$, any energy level is doubly degenerate at a given parity sector, so when doing ELS, we only pick up one of the doubly degenerate levels to demonstrate the GSE. Any small K breaks the degeneracy, then we may consider both sets of energy levels, a small K makes $\langle \tilde{r} \rangle$ small, so

TABLE II: The ELS and degeneracy of the Majorana fermion $q = 4$ SYK model at N even in (a) or odd in (b). The degeneracy d is at a given parity sector $(-1)^{Q_c}$. The total degeneracy d_t is at both parity sectors. (a) When N is even, there is only one anti-unitary operator P . When $N \pmod{8} = 2, 6$, P maps Q_c into $Q_c + 1$. When $N \pmod{8} = 0, 4$, Q_c and $Q_c + 1$ are completely dependent, no operator connects between the two opposite parities. (b) When N is odd, after adding one Majorana fermion at $N + 1 = \infty$, one doubles the Hilbert space, also introduces one more conserved quantity (the parity), there are two anti-unitary operators P and Z . When $N \pmod{8} = 3, 7$, P maps Q_c to itself, Z maps Q_c into $Q_c + 1$. When $N \pmod{8} = 1, 5$, Z maps Q_c to itself, P maps Q_c into $Q_c + 1$. So P and Z exchange their roles in the two cases. So the d_t in the odd N case is the degeneracy in the enlarged Hilbert space which is the twice of the original one⁵³.

$N \pmod{8}$	0	2	4	6
ELS	GOE	GUE	GSE	GUE
β	1	2	4	2
Q	$d = 1$	$d = 1$	$d = 2$	$d = 1$
Q_t	$d_t = 1$	$d_t = 1 + 1$	$d_t = 2$	$d_t = 1 + 1$
$N \pmod{8}$	1	3	5	7
ELS	GOE	GSE	GSE	GOE
β	1	4	4	1
Q	$d = 1$	$d = 2$	$d = 2$	$d = 1$
Q_t	$d_t = 1 + 1$	$d_t = 2 + 2$	$d_t = 2 + 2$	$d_t = 1 + 1$

$\langle \tilde{r} \rangle$ starts from zero and increases as K/J increases, then reaches the GUE in the range from e^{-4} to $e^{0.5}$. There is a CIT from GUE to the Poisson as K/J increases. So in this case, using the NN ELS is not enough. One may start to use the combination of NN and the NNN ELS presented in Sec.2. The $\langle \tilde{r}' \rangle$ was also shown in Fig.3d. It is convenient to combine both $\langle \tilde{r} \rangle$ and $\langle \tilde{r}' \rangle$ into the same Fig.3d. When $\langle \tilde{r} \rangle$ in (d) is close to be zero, the NNN $\langle \tilde{r}' \rangle$ in (d) still shows GSE until $K/J \sim e^{-5}$. When $\langle \tilde{r} \rangle$ in (d) reaches the plateau value ~ 0.60266 of GUE with $\beta = 2$, then according to Eq.10, $\langle \tilde{r}' \rangle$ in (d) reaches the corresponding plateau value listed in Table I as ~ 0.7344 with a RMT index $3\beta + 1 = 7$. When $\langle \tilde{r} \rangle$ in (d) reaches the plateau value ~ 0.38629 of Poisson, according to Eq.10, $\langle \tilde{r}' \rangle$ in (d) reaches a corresponding plateau value listed in Table I as ~ 0.5 . As pointed out in Sec.2, it is only slightly below the GOE value 0.53590 with the RMT index $3\beta + 1 = 1$.

For odd N , due to the absence of the GUE in Table IIb, at the $q = 4$ side, there are only the GSE case in (a) and (d), the GOE case in (b) and (c). They show similar evolution patterns as the corresponding GSE and GOE cases at the $q = 4$ side for even N cases shown in Fig.3.

Obviously, at any given disorder realization of K_{ij} , the eigen-energies of $q = 2$ SYK is in-commensurate (so the disorder in SYK may play a similar role as the Berry phase in the $J - U(1)/Z_2$ Dicke model), a quantum version of Kolmogorov-Arnold-Moser (KAM) theorem⁶⁸ (See Sec V-C) should apply when J/K is sufficiently

small (See Sec V-C). So the ELS changes from the Poisson to GUE around some critical $(J/K)_c$ values. The mean value $\langle \tilde{r} \rangle$ also changes from its Poisson value to the corresponding GUE value. It is similar to the β_c in the $U(1)/Z_2$ Dicke model where the ELS changes from the Poisson to GOE when inside the superradiant phase $g/g_c \geq 1$ (see Fig.2a in⁶⁸). Of course, in contrast to the Dicke model, due to the quenched disorders, there is no regular regime (see Fig.2b in⁶⁸) at any values of J/K . Compared to the ED to study the CIT in the $U(1)/Z_2$ Dicke model, the extra work needed here is that one need to draw the random couplings J_{ijkl}, K_{ij} from the corresponding Gaussian distributions $P[J]$ and $P[K]$, then get ELS at a given set of J_{ijkl}, K_{ij} . Then one need to repeat the same calculations over 40 to 100 samples of such a random realizations of $J_{ij,kl}, K_{ij}$, then perform the average of ELS over these 40 to 100 samples⁵⁵.

One may also understand the quantum analog of the KAM theorem from a dual point of view, namely, the stability of quantum chaos of the quantum chaotic $q = 4$ SYK against the non-chaotic perturbation as one turns on K/J . The dual form of the KAM theorem states that as K/J increases, there should be a crossover from the WD to the GUE, then a CIT from the GUE to the Poisson. Our ED studies shown in Fig.3 and 4 confirms this global picture.

B. The hybrid of $q = 2$ and $q = 4$ complex fermion SYK

The Majorana fermion SYK was extended to the complex fermion which has a $U(1)$ charge symmetry¹⁰. One may also add a chemical potential μ to fix the conserved fermion filling factor⁵⁴:

$$q_c = \sum_i (c_i^\dagger c_i - 1/2) \quad (14)$$

The procedures used for the Majorana fermion in the last subsection (of course, no odd N case anymore) can also be applied to study the $q = 2$ and $q = 4$ type-I hybrid complex SYK:

$$H_C = \sum_{i < j, k < l}^N J_{ij;kl} c_i^\dagger c_j^\dagger c_k c_l + \sum_{i < j}^N K_{ij} c_i^\dagger c_j - \mu q_c \quad (15)$$

where $\langle J_{ij;kl} \rangle = 0, \langle |J_{ij;kl}|^2 \rangle = 3!J^2/N^3$ drawing from the Gaussian distribution $P[J_{ij;kl}] \sim e^{-A|J_{ij;kl}|^2/2J^2}$ where $A = N^3/3!$. In general, $J_{ij;kl} = -J_{ji;kl}, J_{ij;kl} = -J_{ij;lk}, J_{ij;kl}^* = J_{kl;ij}$. We also take the four site indices i, j, k, l are all different⁶⁰ to keep the PH symmetry explicit at $\mu = 0$. $K_{ij}^* = K_{ji}$ is a Hermitian matrix satisfying $\langle K_{ij} \rangle = 0, \langle |K_{ij}|^2 \rangle = K^2/N$.

In the $K/J = 0$ limit, the $q = 4$ complex SYK is non-integrable at any finite N . Under the PH transformation, $q_c \rightarrow -q_c$. So $q_c = 0$ is the PH symmetric and only happens when N is even. At the half-filling $q_c = 0$, the

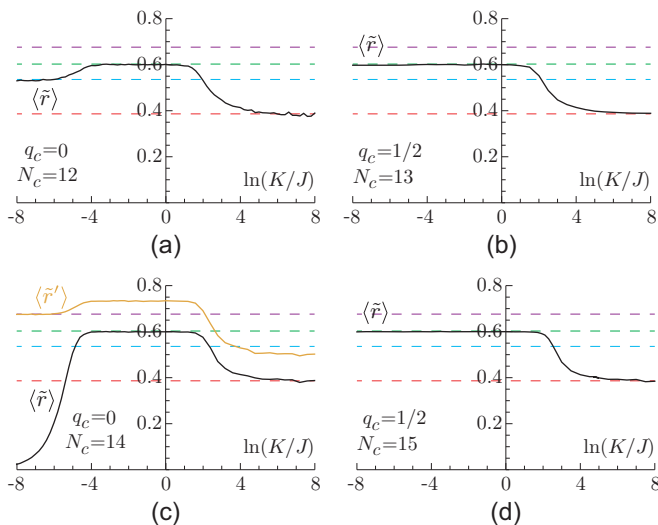


FIG. 5: The evolution of the ELS for type-I hybrid complex SYK model. (a) is GOE (b) and (d) are GUE, (c) is GSE on the $q = 4$ side. $\langle \tilde{r} \rangle$ (black curve), and $\langle \tilde{r}' \rangle$ (orange curve) for GSE case in (c) evaluated at $N_c = 12, 13, 14, 15$ and are averaged over 100, 50, 50, 50 samplings respectively. Note the advantages of using $\langle \tilde{r}' \rangle$ over $\langle \tilde{r} \rangle$ in (c), especially in the quantum chaos side.

system also has the maximum zero temperature entropy s_0^{10} . Away from the half-filling $\mu \neq 0$, it breaks the P symmetry, $-N/2 < q_c \neq 0 < N/2$ corresponds to a non-vanishing electric field in a charged black hole in an asymptotic AdS_2 bulk⁷. It was shown in²³ that when $N \pmod{4} = 0, 2$, the ELS is GOE and GSE respectively. But when $N \pmod{4} = 1, 3$ and $q_c = \pm 1/2$, it is GUE. In fact, as long as $q_c \neq 0$, there is no PH symmetry anymore, so it is in GUE regardless of the value of $N \pmod{4}$.

Now we apply the PH transformation to the hybrid SYK model Eq.15 when $K/J \neq 0$. The fermion number remains to be conserved. However, P is not conserved anymore due to $\{P, H_2\} = 0$ (here and thereafter, H_2 excludes μ in Eq.15). So the hybrid SYK does not have the PH symmetry anymore. Just from symmetry point of view, the hybrid complex SYK belongs to the class A in the 10 fold way classification, so may satisfy GUE for any ratio of K/J . Our ED studies⁵⁷ at a given q_c in Fig.5 shows that this is true only in the intermediate regimes of K/J . The KAM theorem and its dual form applies in the two end regimes $K/J \ll 1$ where the ELS remains Poisson and $K/J \gg 1$ where the ELS becomes the WD determined by the $q = 4$ SYK respectively.

In our ED studies⁵⁷, we first study $q = 4$ SYK to reproduce the known results in²³, then look at the $q = 2$ SYK to show that it indeed satisfies the Poisson distribution. Then we study the hybrid model Eq. 15 at a given q_c at any K/J . The ED result is shown in Fig.5 where there are also 3 cases:

(a) For $N_c \pmod{4} = 0$, at the half filling $q_c = 0$, the hybrid complex fermion SYK is in the GUE in a wide

range near $K/J = 1$, there is a crossover from GOE to GUE, then a CIT from GUE to the Poisson as K/J increases.

(b) Away from the half filling $q_c \neq 0$, regardless of $N_c \pmod{4}$, the $q = 4$ SYK is in GUE. The hybrid complex fermion SYK stays in the GUE across $K/J = 1$ until to $K/J \sim e^{1.5}$, then there is a CIT from GUE to the Poisson as K/J increases further.

(c) For $N_c \pmod{4} = 2$, at the half filling $q_c = 0$, the complex $q = 4$ fermion SYK is in GSE at $K = 0$. Because $P^2 = -1$, any energy level is doubly degenerate, so when doing ELS, we only pick up one of the doubly degenerate levels to demonstrate the GSE at $K/J = 0$. Any small K breaks the degeneracy, then we may need to consider both sets of energy levels, then it is easy to see that any small K makes $\langle \tilde{r} \rangle$ small, so $\langle \tilde{r} \rangle$ starts from zero and increases as K/J increases. The hybrid complex fermion SYK is in the GUE in a wide range near $K/J = 1$. There is a CIT from GUE to the Poisson as K/J increases further.

So in this case, using the NN ELS is not enough. One must to use the combination of NN and the NNN ELS presented in Sec.2. The $\langle \tilde{r}' \rangle$ was also shown in Fig.5c. It is complete to combine both $\langle \tilde{r} \rangle$ and $\langle \tilde{r}' \rangle$ into the same figure. When $\langle \tilde{r} \rangle$ is close to be zero, the NNN $\langle \tilde{r}' \rangle$ still shows GSE until $K/J \sim e^{-5}$. When $\langle \tilde{r} \rangle$ reaches the plateau value ~ 0.60266 of GUE with $\beta = 1$, then according to Eq.10, $\langle \tilde{r}' \rangle$ reaches a corresponding plateau value listed in Table I as ~ 0.7344 with a RMT index $3\beta + 1 = 4$. When $\langle \tilde{r} \rangle$ reaches the plateau value ~ 0.38629 of the Poisson, according to Eq.10, $\langle \tilde{r}' \rangle$ reaches an corresponding plateau value listed in Table I as ~ 0.5 . It is only slightly below the GOE value 0.53590 with the RMT index $3\beta + 1 = 1$.

IV. TYPE II HYBRID SYK MODELS

By Type-II, we mean the integrable side is given by $(q = 2)^2$ SYK which keeps the PH symmetry Eq.12 of the $q = 4$ SYK. We will discuss Majorana and complex type-II hybrid SYK respectively. The results can be contrasted with the corresponding Type-I hybrid SYK models.

A. The particle-hole P or Z conserving hybrid $q = 4$ Majorana fermion SYK

It may also be interesting to study the CIT in the type-II $q = 4$ hybrid Majorana fermion SYK which keeps the PH symmetry at any ratio of K/J :

$$H_{M-II,\pm} = \sum_{i < j < k < l}^N J_{ijkl} \chi_i \chi_j \chi_k \chi_l \pm [i \sum_{i < j}^N K_{ij} \chi_i \chi_j]^2 \quad (16)$$

where J_{ijkl} , K_{ij} are real and satisfy the Gaussian distributions with $\langle J_{ijkl} \rangle = 0$, $\langle J_{ijkl}^2 \rangle = 3!J^2/N^3$ and

$\langle K_{ij} \rangle = 0$, $\langle K_{ij}^2 \rangle = K/N$ respectively. Note that here we use $\langle K_{ij}^2 \rangle \sim K$ to make K/J dimensionless.

Obviously, the second term of $H_{M-II,\pm}$ can be written as H_{M2}^2 . In contrast to Eq.11, it still keeps the P symmetry. So symmetry analysis alone can not distinguish between H_{M4} and H_{M2}^2 despite the former is chaotic, the latter is integrable. Because H_{M2} is integrable, so is H_{M2}^2 . This can be most conveniently seen from the NN ratio $r_n = s_n/s_{n+1}$ of the H_{M2} . Then R_n of the H_{M2}^2 can be written as:

$$R_n = \frac{E_n^2 - E_{n-1}^2}{E_{n+1}^2 - E_n^2} \sim \frac{E_n - E_{n-1}}{E_{n+1} - E_n} = r_n \quad (17)$$

where, similar to the cancelation of the density of states in r_n , the center of two NN energies just cancels in the ratio. Very similarly, one can show that the ratio of the NNN energy spacing $R'_n \sim r'_n$. So the ELS of H_{M2}^2 remains Poisson.

This model with both \pm sign was studied before in²³ by $1/N$ expansion and by the RG analysis at $N = \infty$. By performing the RG on the coefficient of the H_{M2}^2 term around the $q = 4$ SYK conformally invariant fixed point, it was found that the $+$ sign is marginally irrelevant (Fig.9b2), so the $q = 4$ non-integrable SYK NFL fixed point is stable in the IR against the $+H_{M2}^2$ perturbation. However, the $-$ is marginally relevant (Fig.9b1), it flows to the integrable FL fixed point controlled by $-H_{M2}^2$. However, our ED results show that there is very little differences between the two signs in ELS. This fact could be explained as follows:

$$\begin{aligned} -H_{M-II,-}[J, K] &= \sum_{i < j < k < l}^N J'_{ijkl} \chi_i \chi_j \chi_k \chi_l + [i \sum_{i < j}^N K_{ij} \chi_i \chi_j]^2 \\ &= H_{M-II,+}[J', K] \end{aligned} \quad (18)$$

where $J'_{ijkl} = -J_{ijkl}$. So J' and J satisfy the same distribution.

Let E_n^+ be an ordered set of energy levels of $H_{M-II,+}[J, K]$, then $s_n^+ = E_{n+1}^+ - E_n^+ > 0$ are the NN spacings. Then $E_n^- = -E_n^+$ is the corresponding ordered set of energy levels of $H_{M-II,-}[J', K]$ and $s_n^- = E_n^- - E_{n+1}^- = E_{n+1}^+ - E_n^+ = s_n^+$ are the corresponding NN spacings. Similarly, the NNN spacing $s_n'^- = E_{2n-1}^- - E_{2n+1}^- = E_{2n+1}^+ - E_{2n-1}^+ = s_n'^+$. Because (J', K) and (J, K) satisfy the same distribution, so we conclude $H_{M-II,\pm}$ satisfy the same ELS.⁵⁹ This is confirmed by our ED. So we just show our $+$ sign results in Fig.6 and 7. However, there is an exchange between the ground state and the highest energy state in the \pm sign, so the $H_{M-II,\pm}$ will have completely different ground states. This can also be seen by the RG analysis in Fig.9b1,b2²³. This fact may show that the CIT characterized by the RMT at a finite N may be complementary to the QPT characterized by the RG at $N = \infty$. Further elucidations on the intricate relation between RG and RMT will be given in Sec. V.

Because $[P, H_{M-II,\pm}] = 0$ or $[Z, H_{M-II,\pm}] = 0$ (when $N \pmod{8} = 1, 5$, one use Z , in all the other cases, one use

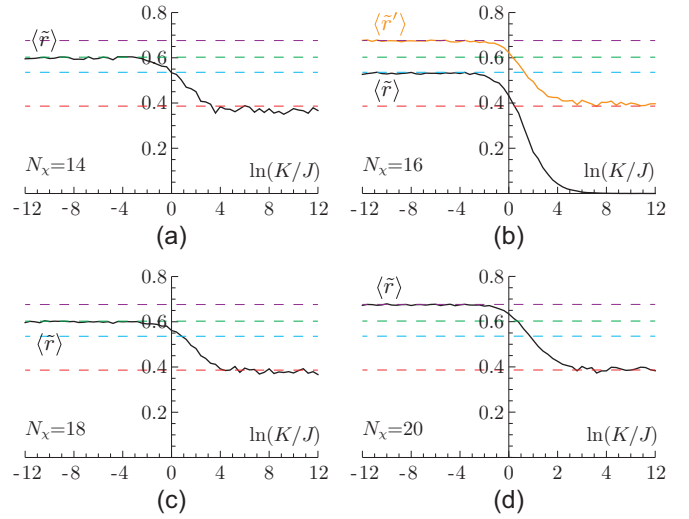


FIG. 6: Even N_x : the evolution of the ELS for type-II hybrid Majorana SYK model when N_x is even. $\langle \tilde{r} \rangle$ (black curve), and $\langle \tilde{r}' \rangle$ (orange curve) in (b) evaluated for $N_x = 14, 16, 18, 20$ and are averaged over 100, 80, 60, 40 samplings respectively. Notably, for $N \pmod{8} = 0$ case in (b), there is a double degeneracy at the $(q=2)^2$ side, the NN ratio $\langle \tilde{r} \rangle$ is rapidly changing near the $(q=2)^2$ side, so it is quite difficult to determine the KAM regime⁶⁸ (See Sec V-C). Fortunately, the NNN ratio $\langle \tilde{r}' \rangle$ shows a nice plateau regime near the $(q=2)^2$ side, the KAM regime can be easily identified and listed in the Table III-VI. This dramatic advantage of the new NNN ratio over the known NN ratio were further demonstrated in all the relevant figures. For $N \pmod{8} = 4$ case in (d), all the energy levels are doubly degenerate at any J/K . The crucial difference between $\langle \tilde{r}' \rangle$ in (b) and $\langle \tilde{r} \rangle$ in (d) are stressed in the text.

P), so symmetry analysis alone can not distinguish between H_{M4} and H_{M2}^2 . So the symmetry classification in Sec.3 still applies to this Type-II hybrid Majorana fermion SYK at any J/K . So the Table II still holds. Our ED studies⁵⁷ in Fig.6 and 7 shows that this is true up to $K/J \sim e^{-2}$. Then the KAM theorem applies at small $J/K \ll 1$ where the ELS becomes Poissonian. There is a CIT from the corresponding WD to the Poisson as K/J increases. However, the degeneracy in Table I remains true at any J/K . In the following, we discuss N even and odd case respectively.

For N even shown in Fig.6, there is always a CIT from the corresponding WD to the Poisson. Several salient features need to be stressed. For $N \pmod{8} = 0$ in (b), one may also look at the ELS from the H_{M2}^2 side when $J/K \ll 1$. Because $\{P, H_{M2}\} = 0$, then $\psi, P\psi$ are still in the same parity sector, but have two different eigenvalues $\pm\lambda$, so are orthogonal. But $[P, H_{M2}^2] = 0$, a pair of orthogonal eigenstates $(\psi, P\psi)$ have the same eigenvalue λ^2 . So H_{M2}^2 is doubly degenerate at $J = 0$. However, the double degeneracy is broken by any $J > 0$. Then using the NN ELS is not enough. One must use the combination of NN and the NNN ELS presented in Sec.2. In contrast to all the previous cases with P or Z violating

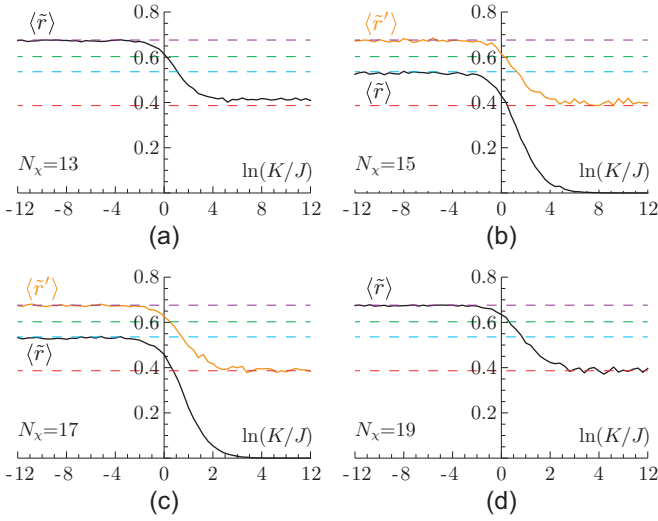


FIG. 7: The evolution of the ELS for type-II hybrid Majorana SYK Model when N_χ is odd. $\langle \tilde{r} \rangle$ (black curve), and $\langle \tilde{r}' \rangle$ (orange curve in (b) and (c)) evaluated for $N_\chi = 13, 15, 17, 19$ and are averaged over 100, 80, 60, 40 samplings respectively. For $N \pmod 8 = 1, 7$ GOE case in (b) and (c), one can see the advantages of using $\langle \tilde{r}' \rangle$ over $\langle \tilde{r} \rangle$, especially in the KAM side. For $N \pmod 8 = 3, 5$ GSE case in (a) and (d), all the energy levels are doubly degenerate at any J/K .

Type-I hybrid SYK models where the doubly degeneracy comes from the $q = 4$ non-integrable side, here the doubly degeneracy comes from the integrable side. It is best to combine $\langle \tilde{r} \rangle$ and $\langle \tilde{r}' \rangle$ in Fig.6b and read them from the $(q = 2)^2$ integrable side. When $\langle \tilde{r} \rangle$ is close to be zero, the NNN $\langle \tilde{r}' \rangle$ still shows Poisson until $J/K \sim e^{-4}$. When $\langle \tilde{r} \rangle$ reaches the plateau value ~ 0.53590 of the GOE with $\beta = 1$, then according to Eq.10, $\langle \tilde{r}' \rangle$ reaches an corresponding plateau value listed in Table I as ~ 0.6769 which is quite close to GSE with a RMT index $3\beta + 1 = 4$.

For $N \pmod 8 = 4$ in (d), there is a CIT from GSE to Poisson as K/J increases. As shown in Table II, there is always a double degeneracy at any J/K . Although $\langle \tilde{r}' \rangle$ in (b) is quite similar to $\langle \tilde{r} \rangle$ in (d), both of which looks like to show a CIT from GSE to Poisson, they have very different physical meanings. As said above, $\langle \tilde{r}' \rangle$ with $N \pmod 8 = 0$ in (b) represents NNN ELS, so it stands for a CIT from GOE to Poisson. While $\langle \tilde{r} \rangle$ with $N \pmod 8 = 4$ in (d) represents NN ELS, so it is a true CIT from GSE to Poisson.

For $N \pmod 8 = 2, 6$ in (c) and (a), there is no degeneracy at any J/K . There is a CIT from GUE to Poisson as K/J increases.

The odd N case is shown in Fig.7. As shown in Table I, one continue to use P symmetry when $N \pmod 8 = 3, 7$, but must use Z symmetry when $N \pmod 8 = 1, 5$. Due to the absence of GUE, there are only two cases: the CIT from GSE to Poisson in (a) and (d) and the CIT from GOE to Poisson in (b) and (c). They show similar evolution patterns as the corresponding CITs for even N case shown in Fig.6. Again, although $\langle \tilde{r}' \rangle$ in (b) and

(c) are quite similar to $\langle \tilde{r} \rangle$ in (a) and (d), both of which looks like to show a CIT from GSE to Poisson, they have very different physical meanings. The former is actually a CIT from GOE to Poisson. While the latter is a true a CIT from GSE to Poisson with a double degeneracy.

B. The particle-hole P conserving hybrid $q = 4$ complex fermion SYK

Now we study the CIT in the following $q = 4$ type-II complex fermion SYK⁵⁴ which also keeps the P symmetry at any ratio of K/J :

$$H_{C-II,\pm} = \sum_{i<j,k<l}^N J_{ij,kl} c_i^\dagger c_j^\dagger c_k c_l \pm \left[\sum_{i<j}^N K_{ij} c_i^\dagger c_j \right]^2 - \mu q_c \quad (19)$$

where $K_{ij}^* = K_{ji}$ is a Hermitian matrix satisfying $\langle K_{ij} \rangle = 0$, $\langle |K_{ij}|^2 \rangle = K/N$. Note that here we use $\langle K_{ij}^2 \rangle \sim K$ to make K/J dimensionless.

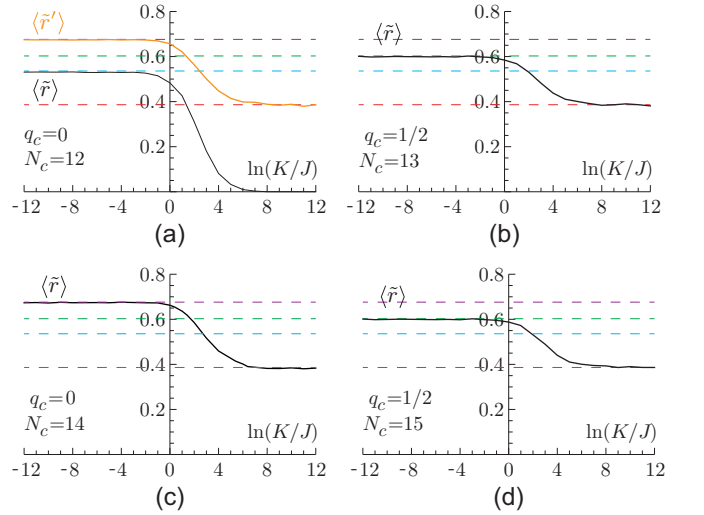


FIG. 8: The evolution of the ELS for type-II hybrid complex SYK model. $\langle \tilde{r} \rangle$ (black curve) and $\langle \tilde{r}' \rangle$ (orange curve) in (a) evaluated with $N_c = 12, 13, 14, 15$ and are averaged over 100, 50, 50, 50 samplings respectively. For $N_c \pmod 4 = 0, q_c = 0$ GOE case in (a), one can see the advantages of using $\langle \tilde{r}' \rangle$ over $\langle \tilde{r} \rangle$, especially in the KAM side. For $N_c \pmod 4 = 2, q_c = 0$ GSE case in (c), all the energy levels are doubly degenerate at any J/K .

Obviously, the second term can be written as H_{C2}^2 . So it still keeps the P and Z symmetry. So symmetry analysis along can not distinguish between H_{C4} and H_{C2}^2 . Then the symmetry classification on complex SYK still applies to this P conserving hybrid $q = 4$ complex fermion SYK. When $N \pmod 4 = 0, 2$ and $q_c = 0$, the ELS is GOE and GSE with the degeneracy $d = 1, 2$ respectively. But when $N \pmod 4 = 1, 3$ and $q_c = \pm 1/2$, it is GUE with the degeneracy $d = 1$. (In fact, as long as $q_c \neq 0$, there is no P symmetry anymore, so it is in GUE

regardless of the value of $N \pmod{4}$). Our ED studies⁵⁷ in Fig.8 shows that this is true until $K/J \sim e^{-1}$. Then the KAM theorem applies at small $J/K \ll 1$ where the ELS becomes Poisson. However, the degeneracy remains true at any J/K . There is a CIT from the corresponding WD to the Poisson as K/J increases.

The rest of discussions are quite similar to the P or Z conserving Type-II hybrid Majorana fermion SYK discussed in the last subsection. Similar to Eq.17, it is easy to show that because H_{C2} is integrable, so is H_{C2}^2 , so its ELS remains Poisson. Furthermore, the eigenvalue of H_{C2}^2 is always positive. Both \pm sign in the second term need to be considered. In the RG sense, we expect the $+$ ($-$) sign in Eq.19 is irrelevant (relevant). However, Eq.18 adopted to Eq.19 shows the ELS stay the same which is confirmed by our ED. So we just show our $+$ sign results in Fig.8. There is always a CIT from the corresponding WD to the Poisson as K/J increases.

Notably, for $N_c \pmod{4} = 0, q_c = 0$ in (a), one may also look at the ELS from the H_{C2}^2 side when $J/K \ll 1$. Because $\{P, H_{C2}\} = 0$, but $[P, H_{C2}^2] = 0$, so H_{C2}^2 is doubly degenerate at $J = 0$. Then using the NN ELS is not enough. One may need to use the combination of NN and the NNN ELS presented in Sec.2. In contrast to the previous P violating type-I hybrid complex SYK model where the doubly degeneracy comes from the $q = 4$ chaotic side, here the doubly degeneracy comes from the integrable side. It is complete to combine both $\langle \tilde{r} \rangle$ and $\langle \tilde{r}' \rangle$ in Fig.a and read them from the $q = 2$ integrable side. When $\langle \tilde{r} \rangle$ is close to be zero, the NNN $\langle \tilde{r}' \rangle$ shows Poisson until $J/K \sim e^{-6}$. When $\langle \tilde{r} \rangle$ reaches the plateau value ~ 0.53590 for the GOE with $\beta = 1$, then according to Eq.10, $\langle \tilde{r}' \rangle$ reaches an corresponding plateau value listed in Table I as ~ 0.6769 which is quite close to the GSE with a RMT index $3\beta + 1 = 4$. There is always a double degeneracy at any J/K in (c). Although $\langle \tilde{r}' \rangle$ in (a) is quite similar to $\langle \tilde{r} \rangle$ in (c), both of which looks like to show a CIT from GSE to Poisson, they have very different physical meanings. As said above, $\langle \tilde{r}' \rangle$ in (a) when $N_c \pmod{4} = 0, q_c = 0$ represents NNN ELS, so it stands for a CIT from GOE to Poisson. While $\langle \tilde{r} \rangle$ in (c) when $N_c \pmod{4} = 2, q_c = 0$ represents NN ELS, so it stands for a CIT from GSE to Poisson and each energy level is doubly degenerate at any K/J .

V. CONTRAST KAM THEOREM OF INTEGRABILITY WITH STABILITY OF QUANTUM CHAOS

In classical chaos, the classical Kolmogorov-Arnold-Moser (KAM) theorem⁶⁸ states that if an integrable Hamiltonian H_0 is disturbed by a small perturbation ΔH , which makes the total Hamiltonian $H = H_0 + \Delta H$, non-integrable. If the two conditions are satisfied: (a) ΔH is sufficiently small (b) the frequencies ω_i of H_0 are in-commensurate, then the system remains quasi-integrable. It plays important roles to study the stability

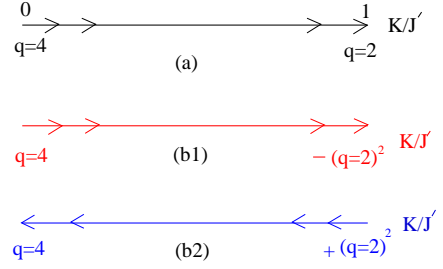


FIG. 9: RG flow of type-I and type-II hybrid SYK models between two different CFT fixed points. (a) The RG flow of the type-I hybrid SYK models. The $K/J', J' = \sqrt{J^2 + K^2}$ is relevant to the $q = 4$ SYK fixed point. So the ground state is always a Fermi liquid (FL) with well defined low energy quasi-particle excitations. (b) Upper, The RG flow of the type-II hybrid SYK models with $-$ sign. The K/J' is marginally relevant to the $q = 4$ SYK fixed point. So the ground state is always a Fermi liquid (FL) with well defined low energy quasi-particle excitations. Lower, The RG flow of the type-II hybrid SYK models with $+$ sign. The K/J' is marginally irrelevant to the $q = 4$ SYK fixed point. So the ground state is always a Non-Fermi liquid (NFL) without the low energy quasi-particle excitations⁹¹.

of solar systems. It remains an outstanding problem to find a quantum analogue of the KAM theorem. Here, we define the quantum analog of the classical KAM theorem as the range of a chaotic perturbation which still keeps the ELS in the Poissonian. The quantum KAM theorem in the context of RMT: For any integrable system subject to a chaotic perturbation, the KAM theorem holds when the chaotic perturbation is below the average many body energy level spacing of the integrable system.

This theorem should hold to any quantum chaotic systems such as hybrid SYK models or Dicke models⁶⁸. Instead of providing a rigorous mathematical proof of this quantum KAM theorem which is left to a future publication⁷¹, we will first give some instructive, but naive estimates which lead to an exponential scaling law, then point out it should be replaced by a large power law. Its precise form may be determined by using more rigorous mathematical treatments⁷⁰ in a future publication⁷¹.

A. Scaling forms of the KAM theorem in the Type-I and Type-II hybrid Majorana or complex SYK

For the hybrid Majorana fermion SYK. The size of the Hilbert space is $2^{N/2}$. On the integrable side, in the $N \rightarrow \infty$ limit, although the single body density of states (DOS) satisfies the semi-circle law, the many body DOS satisfies something similar to a Gaussian which has a variance $\sigma = \sqrt{N/8}$ and also an exponential decay in the two tails (see appendix B), so average bulk many body energy level spacing is $\sim K\sqrt{N/8} \times 2 \times 3/2 \times 2^{-N/2} \sim K\sqrt{N}2^{-N/2}$ where $2/3$ takes care of only $2/3$ states are

within the width $\pm\sigma = \sqrt{N/8}$. Note that the low or high lying spacing is $\sim 1/N$ (which is much larger than the bulk energy level spacing) indicating the existence of the quasi-particles. When doing the ELS, one can simply throw away these low and high energy levels. Because all these many body energy levels are un-correlated and satisfy the Poisson distribution, so naively we expect that when the chaotic perturbation J is smaller than this bulk average spacing, the KAM theorem holds:

$$(J/K)_M \sim \sqrt{N}2^{-N/2} = \sqrt{N}e^{-N \ln 2/2} \quad (20)$$

This scaling seems matche well with the ED results listed in Table III for Type I and Table V for Type II hybrid Majorana SYK. Note that the prefactor \sqrt{N} may not be important in the large N limit, but is important when comparing with the ED data at the sizes we can perform the ED. For example, taking $N = N_\chi = 14$, we can see $J/K \sim 4 \times 2^{-7} \sim 2^{-5} \sim 0.03$ which is quite close to that listed in the Table III. The KAM regime in the other sizes seem also fit the scaling law well. However, as argued below Eq.21, the naive Eq.20 should be replaced by a large power law $\sim 1/N^{\alpha_M}$, $\alpha_M \gg 1$. Unfortunately, the ED at the available sizes may not be able to distinguish the two quite different scaling forms.

For the hybrid complex fermion SYK. Due to the conserved total charge to be $N/2$ at the half filling (other filling can be similar discussed). The size of the Hilbert space is $C_N^{N/2} = \frac{N!}{(\frac{N}{2}!)^2}$. By using Sterling formula $\ln N! = N \ln N - N$ which holds for a large N , one can still show $C_N^{N/2} \sim 2^N/\sqrt{N}$ for a large N . On the integrable side, in the $N \rightarrow \infty$ limit, although the single body density of states (DOS) satisfies the semi-circle law, the many body DOS satisfies something similar to a Gaussian which has a variance $\sigma = \sqrt{N}/4$ and also an exponentially decay in the two tails (see appendix B), so average bulk many body energy level spacing is $\sim K\sqrt{N}/4 \times 2 \times 3/2 \times 2^{-N}\sqrt{N} \sim 3/2KN2^{-N}$. Again, because all these many body energy levels are un-correlated and satisfy the Poisson distribution. so naively we expect that when the chaotic perturbation J is smaller than this average spacing, the KAM theorem holds:

$$(J/K)_C \sim 3/2N2^{-N} = 3/2Ne^{-N \ln 2} \quad (21)$$

In practice, when comparing the data in Table IV for Type I and Table VI for Type II, it is more accurate to use the actual $C_N^{N/2}$ instead of its Sterling form for the sizes we can perform the ED. For example, taking $N = N_c = 12$, then $C_{12}^6 \sim 10^{-3}$, we can see $J/K \sim 6 \times 10^{-3}$ which seems close to that listed in the Table IV and VI. The KAM regime in the other sizes in Table IV and VI seem also fit the scaling law well.

However, as already alerted below Eq.20, the naive Eq.21 should be replaced by a large power law $\sim 1/N^{\alpha_C}$, $\alpha_C \gg 1$. Unfortunately, the ED at the available sizes may not be able to distinguish the two quite different scaling forms. The arguments go as follow: in the integrable side, taking two nearest neighbouring (NN) bulk

states $|B1\rangle = |n_1, n_2, \dots, n_N\rangle_{B1}$ with the eigen-energy $E_{B1} = \sum_i n_i^{B1} \epsilon_i$ and $|B2\rangle = |n_1, n_2, \dots, n_N\rangle_{B2}$ with the eigen-energy $E_{B2} = \sum_i n_i^{B2} \epsilon_i$. The NN means the eigen-energy difference $E_{B1} - E_{B2}$ is of the many-body origin Eq.21. The single particle spacing in the integral side H_2 is $\epsilon_2 - \epsilon_1 \sim K/N$. So $|B1\rangle, |B2\rangle$ must differ by $\sim N/2$ particle occupations n_i to get such a small spacing listed in Eq.21. However, every chaotic perturbation H_4 involves only 4 particle moves in n_i , so typically one need $\sim N/2 \times 1/4 = N/8$ steps to connect the two NN bulk states. The energy of intermediate states involve only 4 single particles, so the change of energy could at most be $4K/N$, then by $N/8$ steps of chaotic perturbation which connects $|B1\rangle$ to $|B2\rangle$, one can estimate the off-diagonal matrix element $\langle B1|H_4|B2\rangle \sim J(J/(4K/N))^{N/8} \sim J(NJ/K)^{N/8}$ which is also exponentially small when $NJ/K \ll 1$. Due to the PH symmetry at the half filling and the self-average in the quenched disorders in the large N limit, one also expect that the diagonal energy shift is tiny $\langle B1|H_4|B1\rangle - \langle B2|H_4|B2\rangle \sim 0$. As argued in⁶⁸, the diagonal energy shift does not lead to the change of ELS anyway. The energy level repulsion is solely due to the off-diagonal matrix element $\langle B1|H_4|B2\rangle$. So we expect the naive Eq.21 should be replaced by a large power law $\sim 1/N^{\alpha_C}$. The large power $\alpha_C \gg 1$ will be determined by a rigorous mathematical derivation in⁷¹. A similar analysis can be applied to the Majorana fermion case to determine the large power α_M in Eq.20.

B. The lower bound of the dual form of the KAM theorem in the Type-I hybrid Majorana or complex SYK

As mentioned in Sec.III-A, one may also study the quantum analog of the KAM theorem from a dual point of view, namely, the stability of quantum chaos of the quantum chaotic $q = 4$ SYK against the integrable perturbation as one turns on K/J . What would be the finite size dependence of the stability of quantum chaos in terms of K/J ? The many body DOS of a RMT satisfies the semi-circle law. However, as shown in the previous works^{9,24,25}, the many body DOS of the $q = 4$ Majorana SYK does not fit the semi-circle law well, but still close to its form near the band edge. The $1/N$ expansion can only get the low end of the DOS which scales as \sqrt{E} . Its whole form can only be achieved by ED. So we use the results in the ED achieved in^{9,24,25}: the bandwidth is $2\epsilon_0^M NJ$ where $\epsilon_0^M \sim 0.05$ is the ground state energy per site in the unit of NJ . Then the average many body energy level spacing is $\sim 2\epsilon_0^M NJ2^{-N/2}$ which defines the Heisenberg time $t_H \sim \frac{1}{NJ}e^N$. Note that the low or high lying spacing is $\sim e^{-s_0 N}$ (which is still much larger than the bulk energy level spacing) indicating the absence of the low energy quasi-particles. In sharp contrast to the KAM theorem in the integral side, all these many body energy levels are correlated and satisfy various WD distributions, so the arguments used to establish the KAM

Eq.20,21 on the integral sides break down. We expect that when the integrable perturbation K is smaller than this average spacing, it remains the same ELS. Naively, the lower bound of the dual form of the KAM takes

$$(K/J)_M > 2\epsilon_0^M N 2^{-N/2} \sim 2\epsilon_0^M N e^{-N \ln 2/2} \quad (22)$$

This lower bound of the scaling seems match well with the ED results for GOE and GSE cases listed in Table III for Type I. For example, taking $N_\chi = 16$, we can see $(K/J)_M > 0.05 \times 32 \times 2^{-8} \sim 6 \times 10^{-3}$ which is indeed below that listed in the Table III. The bound of the dual KAM also seem also fit the other sizes in Table III.

There is a recent $1/N$ evaluation of the many body DOS of the $q = 4$ complex SYK at or away from half-filling which consists of the contributions from both the re-parametrization mode and the $U(1)$ charge mode⁸⁷. Again, this $1/N$ evaluation only captures the physics near to the band edge E_0 of the DOS which was shown to be quite similar to that in the Majorana fermion case, namely the RMT behaviour $\sqrt{E - E_0}$. However, its whole form at the half-filling can only be obtained by the ED which is shown in the appendix C Fig.12: it is quite close to be a semi-circle with the bandwidth $2\epsilon_0^C N J$ where $\epsilon_0^C \sim 0.15$ is the ground state energy per site in the unit of NJ . Then the average many body energy level spacing is $\sim 2\epsilon_0^C N J \sqrt{N} 2^{-N}$. Then Eq.22 can be simply replaced by:

$$(K/J)_C > 2\epsilon_0^C N^{3/2} 2^{-N} \sim 2\epsilon_0^C N^{3/2} e^{-N \ln 2} \quad (23)$$

This lower bound of the scaling seems match well with the ED results for GOE and GSE cases listed in Table IV for Type I. For example, taking $N = 12$, we can see $(K/J)_C > 2 \times 0.15 \times 12 \times 10^{-3} \sim 3.6 \times 10^{-3}$ which is indeed below that listed in the Table IV. The dual form seems also hold in the other sizes in the Table IV.

Due to the strong energy level correlations among the energy levels on the $q = 4$ chaotic side, we expect that the lower bounds Eq.22,23 can be improved significantly. In fact, by using the ETH of the two NN bulk states in the chaotic side in Sec.VI-C, one can show the diagonal energy shift is tiny shown in Eq.28. Again, as argued in⁶⁸, the diagonal energy shift does not lead to the change of ELS anyway. The energy level repulsion is solely due to the off-diagonal matrix element $\langle B_1 | H_2 | B_2 \rangle$ in Eq.29 which need to be evaluated by some rigorous mathematical treatments⁷¹. A similar analysis can be applied to the dual Majorana fermion case.

Of course, Eq.22,23 do not apply to the GUE case for Type I and any case in Type II. In all these cases, there are no changes in ELS from $q = 4$ side to the bulk, there is a direct CIT from the corresponding WD in the $q = 4$ side to the Poisson at the $q = 2$ side. The stability of the quantum chaos does not vanish in the thermodynamic limit.

C. Contrast numerical data with the scaling form of the quantum KAM theorem and its dual form

Now from Fig.3-8 we summarize the stability of quantum chaos near $q = 4$ SYK with the KAM theorem near the integrable $q = 2$ SYK in type-I and $(q = 2)^2$ SYK in type-II in the following 4 Tables from which one can conclude the data support the KAM theorem and the lower bound of its dual form presented in the last subsection.

(1) The validity regime of KAM theorem seem comparable in type-I and type-II. In all the cases, its validity regime gets smaller in exponentially fast as the system size gets larger. These facts are consistent with the KAM theorem in the hybrid SYK models conjectured above.

(2) In type-I, the stability of GOE is comparable to that of GSE. They are also consistent with the KAM in the sizes we studied, also approaches zero as the system's size increases. This is consist with the lower bound of the dual form of the KAM theorem conjectured above. The GOE or GSE will turn into GUE when K/J increases further.

However, the stability of the GUE is much more robust than the two. It is also much more robust than the KAM. This is due to the fact that GUE is dictated by the symmetry classification anyway, so it exists as an intermediate regime in all the three cases, then the stability regime of the GUE at the $q = 4$ side is greatly enhanced. Obviously, it remains a finite value in the thermodynamic limit.

(3) In type-II, the stability of quantum chaos is even among GOE, GUE and GSE. This is because they are dictated by the symmetry classification at the corresponding N values anyway. They are also much more robust than the KAM theorem.

TABLE III: Contrast the stability of quantum chaos at $q = 4$ with the KAM theorem of integrability at $q = 2$ for type-I hybrid Majorana fermion SYK. Notations: N_χ is the number of Majorana fermions, ELS is Energy Level Statistics, QCS is Quantum Chaos stability. KAM is Kolmogorov-Arnold-Moser theorem. The same notations are used in the following tables. The KAM shrinks as the size increases. The QCS of the GUE is greatly enhanced.

N_χ	14	16	18	20
ELS at $K = 0$	GUE	GOE	GUE	GSE
QCS: K/J	$e^0 = 1$	$e^{-5.5} \approx 0.004$	e^0	$e^{-5.5}$
KAM: J/K	$e^{-3} \approx 0.05$	$e^{-3.5} \approx 0.04$	$e^{-4} \approx 0.02$	$e^{-5} \approx 0.01$
N_χ	13	15	17	19
ELS at $K = 0$	GSE	GOE	GOE	GSE
QCS: K/J	$e^{-4.5} \approx 0.01$	$e^{-5} \approx 0.007$	$e^{-5.5} \approx 0.004$	$e^{-5.5}$
KAM: J/K	$e^{-3} \approx 0.05$	$e^{-3.5} \approx 0.04$	$e^{-4} \approx 0.02$	$e^{-5} \approx 0.01$

It remains interesting to test the KAM theorem applied to the hybrid SYK models and its dual form in much large size systems. Unfortunately, the ED can not get to much larger size than $N = 20$ achieved in this paper. In Type-I Majorana fermion hybrid SYK, in the

TABLE IV: Contrast the stability of quantum chaos at $q = 4$ with the KAM theorem of Integrability at $q = 2$ for Type-I hybrid complex fermion SYK. The QCS of the GUE is greatly enhanced.

(N_c, q_c)	(12, 0)	(13, 1/2)	(14, 0)	(13, 1/2)
ELS at $K = 0$	GOE	GUE	GSE	GUE
QCS: K/J	$e^{-5.5} \approx 0.004$	$e^{1.5} \approx 4.5$	$e^{-6} \approx 0.002$	$e^2 \approx 7.3$
KAM: J/K	$e^{-5} \approx 0.008$	e^{-5}	$e^{-5.5}$	e^{-6}

TABLE V: Contrast the stability of quantum chaos at $q = 4$ with the KAM theorem of Integrability at $q = 2$ for Type-II hybrid Majorana fermion SYK. The QCS remains even among all WD and are much more robust than KAM.

N_χ	14	16	18	20
ELS at $K = 0$	GUE	GOE	GUE	GSE
QCS: K/J	$e^{-2} \approx 0.36$	e^{-2}	e^{-2}	e^{-2}
KAM: J/K	$e^{-3} = 0.05$	$e^{-4} = 0.018$	$e^{-5} = 0.007$	$e^{-6} = 0.002$

N_χ	13	15	17	19
ELS at $K = 0$	GSE	GOE	GOE	GSE
QCS: K/J	$e^{-2} \approx 0.36$	e^{-2}	e^{-2}	e^{-2}
KAM: J/K	$e^{-3} = 0.05$	$e^{-4} = 0.018$	$e^{-5} = 0.007$	$e^{-6} = 0.002$

TABLE VI: Contrast the stability of quantum chaos at $q = 4$ with the KAM theorem of Integrability at $q = 2$ for Type-II hybrid complex fermion SYK. The QCS remains even among all WD and are much more robust than KAM.

(N_c, q_c)	12, $q_c = 0$	13, $q_c = 1/2$	14, $q_c = 0$	13, $q_c = 1/2$
ELS at $K = 0$	GOE	GUE	GSE	GUE
QCS: K/J	$e^{-2} \approx 0.14$	e^{-2}	e^{-2}	e^{-2}
KAM: J/K	$e^{-6} \approx 0.002$	$e^{-7} \approx 0.001$	e^{-7}	$e^{-8} \approx 0.0003$

GOE and GSE cases such as Fig.3b,d for even N , Fig.4 for odd N , Type-I complex fermion hybrid SYK, Fig.5a,c, we only identified the KAM theorem from the integrable side and the low bound of its dual form from the quantum chaos side. However, there is no physical understanding on the two ends of the intermediate GUE plateau. The two crossover regimes near the two ends may not satisfy ETH. As alerted at the end of Sec.V-B, in the GUE case (on the $q = 4$ SYK side) of the type-I SYK and all the type-II hybrid SYK models, there is no change from the ELS from the $q = 4$ SYK side to that in the bulk of the hybrid SYK models, so the quantum chaos is always much more robust against an integrable perturbation than the other cases. There is no analytic estimate on the stability regime of this robust quantum chaos. Of course, in contrast to the KAM and its dual form, this robust quantum chaos regime stays robust in the thermodynamic limit.

VI. BULK (OR INTERMEDIATE) STATES CHARACTERIZED BY THE RMT VERSUS EDGE (NAMELY, LOW AND HIGH ENERGY) STATES CAPTURED BY RG OR $1/N$ EXPANSION

It was well established that in terms of symmetries and the space dimension, the RG (including the DMRG, MPS and tensor network) can be used to classify many body quantum phases and quantum phase transitions at $T = 0$ and classical phase transitions at finite temperatures^{62,63}. The RG focus on infra-red (IR) behaviours of the system which are determined by the ground state and low energy excitations. The RG is also intimately connected to general relativity through the holographic principle³³. RG is usually applied to a system in the thermodynamic limit to characterize the quantum phase transitions (QPT). When it gets to a finite system, finite size scalings near the QCP can be used to extract the information at a finite N from the knowledge at $N = \infty$. For a zero dimensional system such as SYK models or $U(1)/Z_2$ Dicke models⁶⁸ with infinite-range interaction, one can use a $1/N$ expansion to study the similar properties.

While the 10-fold way RMT classification scheme to describe quantum chaos in a many body system only depends on two anti-unitary or one unitary chiral operators, seems independent of space dimension. It covers all the energy levels of the system, so can be used to characterize the CIT. RMT is usually applied to a system with a finite size N . In a completely different context, the 10-fold way can also be used to classify topological equivalent class for non-interacting (single particle) topological insulators and topological superconductors⁴⁸⁻⁵⁰. In this case, it also depends on the space dimension and has the Bott periodicity $d \rightarrow d + 8$.

A. QPT versus CIT

The differences and connections between RG at $N = \infty$, then a $1/N$ expansion at a finite N and the RMT at a finite N are explicitly demonstrated in the two types of SYK models in this work. For example, in the thermodynamic limit $N = \infty$, the fermions in the type-I hybrid SYK models have scaling dimension $1/2$ and $1/4$ at the $q = 2$ and $q = 4$ SYK respectively. So the $q = 2$ ($q = 4$) SYK is a stable (unstable) conformally invariant fixed point (Fig.9a). Any J (K) is irrelevant (relevant) to the $q = 2$ ($q = 4$) SYK. At any $K/J \neq 0$, the ground state is controlled by the $q = 2$ SYK fixed point, so it is always a non-chaotic Fermi liquid with well defined low energy quasi-particle excitations. There is no quantum phase transition (QPT) in the type-I hybrid SYK models. There is no finite temperature transitions either. However, as shown in Fig.3-8, there is always a chaotic to integrable transition (CIT) from the GUE to Poisson. Of course, the name of CIT need to be interpreted correctly, because it is dramatically different than

a QPT, The former is characterized by RMT, the latter is by RG or $1/N$ expansion. As shown in these figures, if there is a symmetry change from the $q = 4$ SYK to the hybrid SYK, there are also crossovers between different WD ensembles as K/J increases.

Quantum or topological phase transitions always start from the zero temperature $T = 0$, then raise up to a low temperature $1 \ll \beta J < N$. Especially one can find scaling functions for various physical quantities near the QPT⁶³. If putting the system at a finite size, one may also do finite size scaling to identify the QPT by numerical simulations. It is a bottom/up approach. On the other hand, the Quantum chaos can only happen at non-zero temperature. In fact, it could even start from the infinite temperature $T = \infty$, then lower down to the low temperature $1 \ll \beta J < N$. So it is a top/down approach. Therefore the two approaches are complementary to each other.

QPT only involves the change of the ground states and the low energy excitations, while the high energy states are irrelevant. There is a divergent length scale (the time scale is related to the length scale by a dynamic exponent z) and associated scalings near a QPT in the thermodynamic limit $N = \infty$. While the ELS involves the bulk energy levels at a finite but large enough N , the low or high energy levels are irrelevant (see appendix D). So the QPT characterized by RG and the CIT characterized by the RMT are dramatically different, but complementary to each other. Despite the absence of QPT in the two types of the hybrid SYK models presented in Sec.III and IV respectively, there could still be a CIT which is dramatically different than QPT. There is no divergent length (or time) scales, no associated scalings, therefore no finite size scalings near a CIT⁷³, but there is a KAM in the integrable side and its dual form in the chaotic side if there is a change of level statistics as presented in Sec.V.

In the Type-II hybrid SYK models, the coefficient of $(q = 2)^2$ is marginally irrelevant/relevant when the sign is $+/-$ (Fig.9b). So the ground state with $+$ sign is the non-Fermi liquid without quasi-particle excitations controlled by $q = 4$ SYK fixed point, while that with $-$ sign is the Fermi liquid with well defined quasi-particle excitations controlled by $(q = 2)^2$ SYK fixed point⁶¹. There is no quantum phase transition (QPT) and no finite temperature transitions either in the type-II hybrid SYK models. However, independent of the $+/-$ sign, there is always a CIT from the corresponding WD of $q = 4$ SYK to the Poisson as shown in Fig.6,7 and 8. In fact, as explained in Sec.3.3,3.4, despite the $+/-$ sign leads to dramatically different ground states, the ELS is identical⁵⁹. So here we provide an interesting example where the ELS are the same, but the ground states are dramatically different⁹¹. This fact demonstrates explicitly the dramatic differences between the two classification schemes which are complementary to each other, the RG focus on the ground state and low or high energy excitations, while the RMT focus on the bulk high energy levels (see appendix D).

For another example, as shown in appendix A, the ground states of the hybrid bosonic SYK is a quantum spin glass which breaks ergodicity. There is a finite temperature phase transition at $T = T_{QSG}$ from the QSG to a paramagnet where the ergodicity is restored. However, as shown in Fig.10 in the appendix A, the ELS stays as GOE or GUE. There is no CIT. In order to probe the quantum spin glass ground state at $T < T_{QSG}$, one need to focus on the low energy excitations which, as alerted above, can not be described by the RMT, need to be investigated by RG or $1/N$ expansion.

In any cases, the RMT of the bulk states are quite insensitive to these edge (low or high energy) states⁸⁹. Namely, when evaluating the ELS, incorporating or throwing away these edge states will not affect the ELS. To see these edge states, RG or $1/N$ expansion may be used to study the ground state and its low or high energy excitations. In fact, as outlined in the introduction, using $1/N$ expansion, many previous works studied the conformably invariant QSL and also its extensive low energy excitations with the energy spacing $\sim e^{-s_0 N}$ which leads to the zero temperature entropy s_0 (taking $T \rightarrow 0$ limit after taking $N \rightarrow \infty$ limit which belongs to the regime (b) in the following subsection).

B. Remarks on Lyapunov exponents from OTOC and SFF in the hybrid SYK models

As stressed in the conclusion of Ref.²⁸, there are at least two completely ways to characterize the quantum chaos. One way is through evaluating the regulated out-of-time-ordered correlation function (OTOC). Another way is to use the RMT to characterize the quantum chaos at a very late time. As demonstrated in all the previous sections, when collecting the ELS of the bulk energy levels, low and high energy levels can be simply thrown away without affecting the bulk ELS (see appendix D). So the two ways are complementary to each other.

The OTOC of the two bosonic or fermionic Hermitian operators $V^\dagger = V, W^\dagger = W$ is defined by:

$$F(t) = Tr[yW^\dagger(t)yV^\dagger(0)yW(t)yV(0)] \quad (24)$$

where $y = e^{-\beta H/4}/Z^{1/4}$ is one quarter of the density matrix and $Z(\beta) = Tre^{-\beta H}$ is the partition function. In the SYK models, $V = W = \psi$ or c for Majorana or complex SYK respectively. Its early time exponential growth can be characterized by a quantum Lyapunov exponent, while its late time approaches a constant, so become featureless. The early time behaviour is mainly determined by the ground state and the low energy excitations, while the bulk energy levels are irrelevant (see appendix D). The OTOC reflects the ground state and low energy excitations, so it is directly related to the RG description and can be addressed by $1/N$ expansion. It seems quite insensitive to the 10-fold way global discrete symmetry classification, therefore independent of $N \pmod{8}$ or $N_c \pmod{4}$.

For the $q = 4$ Majorana SYK model, as shown in¹³, at any finite temperature, one must consider the effects of the finite temperature βJ versus the finite size N . (a) At very low temperatures $\beta J > N$, the OTOC takes a power law $\sim t^{-6}$ in the long time limit $t_H > t > \beta > N/J$, so the Lyapunov exponent λ_L can not even be defined at such a low temperature. (b) At intermediate temperatures $1 < \beta J < N$, then the OTOC takes the exponential form in the early time upto the Ehrenfest (or the scrambling time $t_s \sim \beta \log N$) which defines the Lyapunov exponent λ_L , but still decays as $\sim t^{-6}$ in the long time limit $t_H > t > N/J > \beta$. (c) In the high temperature range $\beta J < 1 \ll N$, the physics seems dominated by the microscopic energy scale J , the Lyapunov exponent $\lambda_L \sim J$.

It remains interesting to study how the K term changes the behaviours of the OTOC and the associated Lyapunov exponent λ_L at all the three temperature regimes (a),(b) and (c). In both types of hybrid SYK models, the three temperature regimes are still determined by the competition between the finite size N and the finite temperatures, so adding a K term will not change such a division. (a) is still not the regime to even define a Lyapunov exponent, so we only need to focus on (b) and (c). In the regime (b) $1 \ll \beta J < N$. We expect that for both type I and type II hybrid SYK models, the Lyapunov exponent $\lambda_L > 0$ can be also computed in all the quantum chaotic regimes defined in the RMT sense. We expect $\lambda_L = 0$ in the KAM regime. In the regime (c), we expect that in the quantum chaotic side, any small K will reduce the Lyapunov exponent to $\lambda_L \sim J - K + \dots$. It will vanish in the KAM regime. Because at such a high temperature, all the energy levels are involved, so we expect there may exist a one to one correspondence between λ_L and the KAM theorem from the RMT in the regime (c).

As said in the introduction, in addition to the ELS in the RMT classifications, the CIT may also be dynamically diagnosed from the spectral form factor (SFF)^{25,35}:

$$g(t, \beta) = \frac{\langle Z(\beta, t) Z^*(\beta, t) \rangle_J}{\langle Z(\beta) \rangle_J^2} \quad (25)$$

where $Z(\beta, t) = \text{Tr}(e^{-(\beta+it)H})$ and the disorder average was taken separately in the numerator and denominator.

The SFF at $1 < \beta J < N$ may also be used to measure the dynamic (time-dependent) chaotic behaviours of the two types of hybrid SYK models. A slope-dip-ramp-plateau structure in the time evolution was considered to be evidence for the chaotic behaviours. This feature should disappear in the KAM regime. It remains interesting to study its evolution in the quantum chaotic regime in both regimes (b) and (c).

The constraints of the symmetries P in Eq.12 and Z in Eq.13 put on the OTOC Eq.24 and the SFF 25 will also need to be explored.

C. Remarks on Eigenstate Thermalization hypothesis (ETH): its power on bulk states and inability to encode the edge states

It is interesting to note that the RMT was originally proposed to study statistically the many body energy level correlations of a nuclei with a large atomic number to hold large number of electrons^{76,77}. Then it was used to classify the quantum chaos of non-interacting electrons moving in a random potential which may show metal to Anderson insulator transition⁷⁸. There is a corresponding Chaotic to Integrable transition (CIT) where *the single particle* ELS satisfies WD in the metal, while Poisson in the Anderson insulator.

Recently, there is a renewed interest on Eigenstate Thermalization hypothesis (ETH) in many body interacting systems⁴³. It states that for any excited (also called bulk) state $|\psi\rangle$ with eigen-energy E which is above the ground state energy by a finite amount in the thermodynamic limit: $\lim_{V \rightarrow \infty} \frac{E - E_0}{V} \neq 0$, one may define a temperature β corresponding to the state: $\langle \psi | H | \psi \rangle = \text{Tr} H e^{-\beta H} / Z$ where $Z = \text{Tr} e^{-\beta H}$ is the partition function, then ETH implies than for any local operator O :

$$\langle \psi | O | \psi \rangle = \text{Tr} O e^{-\beta H} / Z \quad (26)$$

The entanglement entropy of the excited state $|\psi\rangle$ satisfies the volume law, while that of the ground state or all the low energy states satisfy the more common area law.

Noow one can use Eq.26 to evaluate the diagonal energy level shift on the chaotic side due to the integrable perturbation $O = H_2$. Taking the complex SYK model at half-filling for an example, assuming the temperatures corresponding to the two NN bulk state $|\psi_1\rangle, |\psi_2\rangle$ in the chaotic side are β_1, β_2 , then one can see:

$$\langle \psi_1 | H_4 | \psi_1 \rangle - \langle \psi_2 | H_4 | \psi_2 \rangle = \frac{1}{Z} \text{Tr} H_4^2 e^{-\beta_1 H_4} \delta\beta \quad (27)$$

Equating Eq.27 to Eq.23 leads to $\delta\beta = \beta_1 - \beta_2 \sim N^{3/2} 2^{-N}$. Then one can immediately see the diagonal energy level shift:

$$\begin{aligned} \langle \psi_1 | H_2 | \psi_1 \rangle - \langle \psi_2 | H_2 | \psi_2 \rangle &= \frac{1}{Z} \text{Tr} H_2 H_4 e^{-\beta_1 H_4} \delta\beta \\ &\sim N^{3/2} 2^{-N} \end{aligned} \quad (28)$$

which is very tiny. Then one may focus on the off-diagonal matrix element $\langle \psi_1 | H_2 | \psi_2 \rangle$. By using the Cauchy inequality $|\langle \psi_1 | O | \psi_2 \rangle|^2 < \langle \psi_1 | O | \psi_1 \rangle \langle \psi_2 | O | \psi_2 \rangle$, one can establish the bound:

$$|\langle \psi_1 | H_2 | \psi_2 \rangle| < \text{Tr} H_2 e^{-\beta_1 H_4} / Z \quad (29)$$

which maybe useful to evaluate the dual form Eq.23 in Sec. V.

Because ETH focus on excited states, so it should be closely related to RMT. Indeed, for interacting many body systems, the quantum chaos imply the ETH or vice versa⁴³. The results achieved in this paper show that

the ETH of $q = 4$ SYK should be preserved in all the plateau regimes in Fig.3-8 satisfying a WD class in the hybrid SYK models. While the KAM theorem implies the violation of ETH or broken ergodicity. The transition regimes between different plateaus may not satisfy ETH either.

The ETH only applies to the bulk states, so it has a very serious limitation: it has no saying on ground state and the low energy excitations which can be defined as $\lim_{V \rightarrow \infty} \frac{E-E_0}{V} = 0$. They are nothing but the edge states. So the conjecture that a single bulk eigenstate encodes the information of the full Hamiltonian⁴⁴ clearly fails on the edge states. A complete understanding of the system needs not only the knowledge of the bulk states in a statistics way by a RMT, but also the edge states by more quantitative approach such as $1/N$ expansion or RG.

D. Comments on some early works on type-I hybrid Majorana SYK models

In this section, we comment on previous works^{73,74} on the type-I hybrid SYK model and also point out their main differences than our work.

The special GUE case (a) and (c) in Fig.3 (but not the other two cases of GOE in (b) and GSE in (d)) in type-I Majorana fermion hybrid SYK Eq.11 at even N was studied in⁷³. However, the most interesting case of the interruption of GUE in the intermediate ranges of K/J in the other two cases (b) and (d) is absent in this special GUE case (a) and (c). Furthermore, these authors in-correctly interpret the CIT as a true QPT at $T = 0$ or a classical phase transition at $T > 0$. So it does not correspond to the Hawking-Page transition in its bulk gravity dual as claimed in this work. It was known that the Hawking-Page transition in the bulk may be dual to a true quark-gluon confinement to deconfinement transition at $T > 0$ in the boundary. The dramatic differences between the CIT characterized by RMT at a finite N and a true quantum or a classical phase transitions characterized by RG at $N = \infty$ was stressed in the last subsection. The finite size scalings to locate a quantum critical point (QCP) only apply to the later, not to the former. Unfortunately, the authors in⁷³ still tried to fit their data to a finite size scaling without success.

After submitting the first version of our work to arXiv, we got to know the authors in⁷⁴ have also studied the other two cases of (b) and (d). Furthermore, they also evaluated the Thouless energy scale $E_{th} = N^2 \Delta$ where Δ is the average many body energy level spacing beyond which the RMT breaks down²⁴. However, this reference did not (1) introduce the new NNN ratio r' (2) do the odd N case (3) study the type II cases (4) address the possible deep relations between the RG at $N = \infty$, $1/N$ expansion at a finite N and the RMT at a finite N . As shown in Sec.III-A, Sec.IV-A, the odd number of sites are in different classes in both classifications and ED⁵³. In

the GSE case in Fig.3-5, which has the double degeneracy at the $q = 4$ side, the new NNN ratio r' must be used to describe the stability regime of the quantum chaos in the GSE side and also describe the whole crossover from GSE to the GUE, then the CIT from GUE to the KAM side with the Poisson distribution. The new NNN ratio must be used to describe the KAM theorem in the integrable side when there is a double degeneracy in the integrable side as are the cases in Fig.6b, Fig.7b,c and Fig.8a in the type-II hybrid SYK models.

VII. CONCLUSIONS AND PERSPECTIVES

RG is a semi-group which may not have an inverse. In the coarse graining process, some information gets lost, the self similar phenomena start to emerge only in the low energy limit. What kind of information is lost ? We believe what is lost is the RMT information. It is worth to point out that in relativistic quantum field theories, the low energy and high energy levels are closely related due to the Lorentz invariance. So the RG can be equivalently performed by removing the IR or UV divergencies. This procedure is well established by the dimensional regularization in relativistic quantum field theories. It has also been applied to non-relativistic quantum field theories to describe the superfluid to Mott transition⁷⁹ with the long range Coulomb interaction and also the quantum Hall plateau-plateau transition in a periodic potential with the long range Coulomb interaction^{80,81}. We expect the bulk energy levels of these systems are also described by the RMT. Similarly, the QCD is described by the asymptotical freedoms in the high energy (or short distance) limit, but its bulk energy levels are described by the RMT⁸²⁻⁸⁴.

Here we introduced a new universal ratio which is the ratio of the next nearest neighbour (NNN) energy level spacing to characterize the random matrix behaviours. It must be used when there is a double ($d = 2$) degeneracy near the chaotic side or near the integrable side. This new universal ratio is particular useful when numerically characterizing the KAM regime in the integrable side and the stability of quantum chaos in the chaotic regime. In Sec.V, we only present some very preliminary results on the analytical scaling forms of the KAM and its dual form. Their complete and rigorous forms will be given in a separate publication⁷¹. If there are higher order such as $d = 3, 4, \dots$ degeneracy such near the chaotic side or near the integrable side, then one may need to introduce more universal ratios such as the NNNN, NNNNN ratios or the whole series whose physical meanings remain to be explored. This is similar to Tensor category, upto higher order tensor category are needed to characterize the topological phases³⁴.

In a recent work⁷⁵, we studied quantum chaos in 2- or 4-colored SYK models and also CIT in 2- or 4-colored hybrid SYK models. These colored SYK models provide concrete examples of classifying quantum chaos in a sys-

tem with multiple conserved quantities which show richer RMT classes⁸⁵ than the conventional SYK models. The NNN ratio should also find its applications in numerically studying KAM and its dual form in the 2- or 4-colored hybrid SYK models. It may also be interesting to study the ELS of the two indices SYK model⁶⁹ with the two large numbers: N (the number of sites) and the M (the group of $O(M)$ or $SU(M)$). Depending on the relations between N and M , it may show either chaotic QSL or symmetry-broken QSG ground state.

As shown in⁴⁵, the stability of quantum chaos of black holes against a constant $q = 2$ SYK terms may be used to explore the interior behind the black hole horizon. Implications of the results achieved here on the bulk gravity side or on quantum error corrections to AdS/CFT need to be explored⁷².

Fig.9b1 and Fig.9b2 show that the $q = 4$ chaotic SYK CFT fixed point and the $(q = 2)^2$ integral CFT flow towards each other with \pm sign respectively. In 2d CFT, Zamolodchikov's c-theorem states that RG flows only from a CFT with central charge c_1 to another one with $c_2 < c_1$. One can construct a c-function which monotonically decrease from c_1 to c_2 . The 2d C-theorem can also be extended to higher dimensions through F-theorem in odd dimension or a-theorem in even dimension³³. In the 2d boundary CFT (BCFT), there is a also a g-theorem³⁶⁻⁴⁰ which states that there is only one way RG flow from a BCFT with the boundary degeneracy g_1 to another one with $g_2 < g_1$. However, there is no such a c-theorem in a 1d CFT. This maybe special to the 1d CFT where one can only associate a Lyapunov exponent λ_L when away from the CFT due to a leading irrelevant operator (so called NCFT₁) instead of a central charge c to a CFT fixed point. This may also be related to the distinction of $NAdS_2/NCFT_1$ from its higher dimension counterparts. It remains important to explore further the possible deep mechanism on the two ways RG flow between the FL and NFL fixed points in 1d CFT.

Acknowledgments

J. Ye thank C. Xu for helpful discussions. F.S and J.Y thank Prof. Gang Tian and Prof. Congjun Wu for the hospitality during their visit at the West Lake university; also thank Prof. Wei Ku for the hospitality during their visit at the Tsung Dao Lee Institute in Shanghai, China. F.S and J.Y acknowledge AFOSR FA9550-16-1-0412 for supports. Y.Y thank Y.-Z. You for sharing the ED code used in Ref.²³. This research at KITP was supported in part by the National Science Foundation under Grant No. NSF PHY-1748958. WL was supported by the NKBRSCF under grants Nos. 2011CB921502, 2012CB821305, NSFC under grants Nos. 61227902, 61378017, 11311120053.

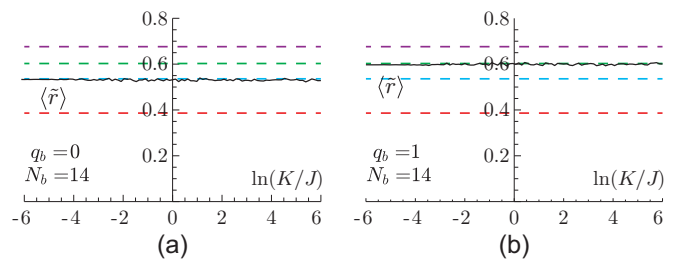


FIG. 10: ELS of the hybrid bosonic SYK. (a) For N_b even, at the half filling $q_b = 0$, it is always in GOE for any ratio of K/J . (b) Away from the half filling $q_b \neq 0$, it is always in GUE for any ratio of K/J , regardless of N_b is even or odd. In contrast to the fermion cases presented in the main text, there is no CIT in the bosonic hybrid SYK. However, it is not known if there is a QPT between the bosonic QSG₂ and QSG₄ in the ground state.

Appendix A: The hybrid of $q = 2$ and $q = 4$ bosonic SYK

This appendix was cited in Sec.VI-A. The procedures for fermions presented in the main text can also be applied to study the $q = 2$ and $q = 4$ hybrid bosonic SYK:

$$H_B = \sum_{i < j, k < l}^N J_{ij;kl} b_i^\dagger b_j^\dagger b_k b_l + \sum_{i < j} K_{ij} b_i^\dagger b_j - \mu q_b \quad (\text{A1})$$

where, in general, $J_{ij;kl} = J_{ji;kl}$, $J_{ij;kl} = J_{ij;lk}$, $J_{ij;kl}^* = J_{kl;ij}$ and $\langle |J_{ij;kl}|^2 \rangle = 3!J^2/N^3$. $q_b = \sum_i (b_i^\dagger b_i - 1/2)$ is just the boson analog of Eq.14. Following¹⁰, we take the four site indices i, j, k, l are all different⁶⁰ to keep the PH symmetry explicit at $\mu = 0$. $K_{ij}^* = K_{ji}$ is a Hermitian matrix satisfying $\langle K_{ij} \rangle = 0$, $\langle |K_{ij}|^2 \rangle = K^2/N$.

In the $K/J = 0$ limit, the $q = 4$ bosonic SYK was studied by the ED in¹⁰, a Quantum spin glass (QSG) ground state was expected in the thermodynamic limit $N = \infty$. One can define the particle-hole symmetry operator to be $P = K \prod_{i=1}^N (b_i^\dagger + b_i)$. The boson charge operator is $Q_b = \sum_i b_i^\dagger b_i$. It is easy to show $P^2 = 1$, $P b_i P = b_i^\dagger$, $P b_i^\dagger P = b_i$, $P Q_b P = N - Q_b$. $[P, H_{M4}] = 0$. For N even, at half filling $q_b = 0$, it is in GOE. However, as long as $q_b \neq 0$, there is no PH symmetry anymore, it is in GUE regardless of the value of N is even or odd.

Now we apply the PH transformation to the bosonic hybrid SYK model Eq.A1. In contrast to the fermionic hybrid SYK models, $[P, H_2] = 0$, so the PH symmetry is preserved in the hybrid bosonic SYK model. In the $J/K = 0$ limit, we expect that the ELS for $q = 2$ bosonic SYK is the same as $q = 4$ bosonic SYK: when $q_b = 0$, it is in GOE, when $q_b \neq 0$, it is in GUE. This is in sharp contrast to the $q = 2$ fermionic SYK which is non-interacting, so integrable. While the $q = 2$ bosonic SYK is interacting (the bosons on the same site behaves as fermions, but different sites as bosons), so non-integrable and is already a quantum chaotic system.

So we expect the ELS of the hybrid bosonic SYK stays the same from $q = 4$, all the way down to $q = 2$. This is indeed confirmed by our ED results⁵⁸ shown in Fig.10, there are only two cases here (a) For N_b even, at the half filling $q_b = 0$, it is always in GOE for any ratio of K/J . (b) Away from the half filling $q_b \neq 0$, it is always in GUE for any ratio of K/J , regardless of N_b is even or odd.

In short, in contrast to all the hybrid fermionic models discussed in the main text, the KAM theorem does not apply in the bosonic hybrid model where there is no CIT. Here we only focused on the ELS of bulk spectrum. It supports the claim made in Sec.VI-A on the relation between the edge versus bulk energy levels and belong to the class A in the BSCFS.

Appendix B: The many-body density of states of $q = 2$ Majorana and $q = 2$ complex SYK models

In this appendix, we provide the many body energy distributions of the $q = 2$ Majorana and $q = 2$ complex SYK models which are needed to derive the scaling forms of the KAM theorems for the corresponding hybrid SYK models in Sec. V. Surprisingly, there is no previous works to discuss the many body energy level distributions of the $q = 2$ Majorana or complex SYK models.

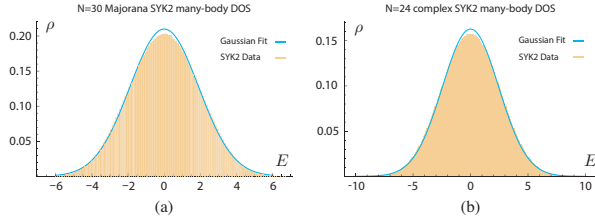


FIG. 11: The Many-body density of states of $q = 2$ Majorana and complex SYK models: (a) Majorana fermion case at a given parity (b) complex fermion case at half-filling. Both many body DOS are close to be a Gaussian distribution with a small deviation in the center⁹⁰. However, it is difficult to resolve the precise nature of the band edge numerically.

1. $q = 2$ Majorana SYK model.

The $q = 2$ Majorana SYK model in Eq.11 is defined as $H_\chi = i \sum_{1 < i < j \leq N} K_{ij} \chi_i \chi_j$, where K_{ij} is real random number and drawn from the Gaussian distribution with zero mean and K^2/N variance. So its single particle energy levels fit rigorously the RMT description¹¹ with the matrix size $L = N$.

One can calculate its all many-body energy levels $\{E_\chi\}$ at a given parity sector by diagonalizing a $2^{N/2-1} \times 2^{N/2-1}$ sparse matrix (assuming N is even). Obviously, $\langle E_\chi \rangle = 0$. The data $\langle E_\chi^2 \rangle$ is listed in Table VII. We find that the many-body energy level statistics (ELS) is a Poisson and the many-body energy density of states (DOS) $\rho(E_\chi)$ satisfies a Gaussian distribution with zero mean and variance $\sigma^2 = 0.127N - 0.157 \approx N/8$. This value matches the analytic estimate of the second mo-

ment $TrH^k/Tr1 = [\frac{\langle J^2 \rangle}{2q} C_N^q]^k / 2^{25}$. Putting $k = 2, q = 2$ and $\langle K^2 \rangle = K^2/N$, we find it is $K^2N/8$. The fitted Gaussian distribution and $\rho(E_\chi)$ are shown in Fig.11a.

TABLE VII: The $\langle E_\chi^2 \rangle$ of the $q = 2$ Majorana SYK in the even parity sector averaged over 1000 samples. We choose $K = 1$ to perform the ED. The data of $\langle E_\chi^2 \rangle$ show a linear dependence on N , and give $\langle E_\chi^2 \rangle = 0.127N - 0.157$.

N_χ	12	14	16	18	20
$\langle E_\chi^2 \rangle$	1.354	1.631	1.864	2.129	2.397
N_χ	22	24	26	28	30
$\langle E_\chi^2 \rangle$	2.624	2.887	3.085	3.391	3.665

2. $q = 2$ Complex SYK model.

The $q = 2$ complex SYK model in Eq.14 is defined as $H_c = \sum_{1 \leq i < j \leq N} K_{ij} c_i^\dagger c_j$, where $K_{ij} = K_{ji}^*$ is random complex number drawn from the Gaussian distribution with $\langle K_{ij} \rangle = 0$ and $\langle |K_{ij}|^2 \rangle = K^2/N$. The fermion number $Q_c = \sum_i c_i^\dagger c_i = q$ is conserved. So its single particle energy levels fit rigorously the RMT description¹¹ with the matrix size $L = N$.

One can calculate its all many-body energy levels $\{E_c\}$ in the half-filling sector ($q = N/2$ for N even) by diagonalizing a $C_N^{N/2} \times C_N^{N/2}$ sparse matrix (assuming N is even). Obviously, $\langle E_c \rangle = 0$. The data of $\langle E_c^2 \rangle$ is listed in Table VIII. We find the many-body ELS is a Poisson and many-body energy DOS $\rho(E_c)$ satisfies a Gaussian distribution with zero mean and $\sigma^2 = 0.250N + 0.002 \approx N/4$ variance. The fitted Gaussian distribution and $\rho(E_c)$ are shown in Fig.11b.

TABLE VIII: The $\langle E_c^2 \rangle$ of the $q = 2$ complex SYK at half filling averaged over 10000 samples. We choose $K = 1$ to perform the ED. The data of $\langle E_c^2 \rangle$ show a linear dependence on N , and give $\langle E_c^2 \rangle = 0.250N + 0.002$.

N_c	10	12	14	16
$\langle E_c^2 \rangle$	2.499	3.001	3.501	4.001
N_c	18	20	22	24
$\langle E_c^2 \rangle$	4.501	5.004	5.503	5.998

Appendix C: The many-body density of states of $q = 4$ complex SYK models

The many body DOS for the $q = 4$ Majorana SYK was studied by $1/N$ in⁹ and ED in²⁵. It was found that globally it is like Gaussian with the variance $\sqrt{J^2 N/64}$, locally look like the semi-circle DOS with $\sqrt{E - E_0}$ behaviour near the band edge (either low or high). The many body DOS for the $q = 4$ complex SYK is shown in Fig.12.

At fixed $q = 4$, as N gets large, the many body DOS of Majorana or complex SYK globally approaches the

Gaussian with a width $\sigma \sim \sqrt{N}$. However, near the band edge $E_0 \sim N$, it shows the $\sqrt{E - E_0}$ behaviour. So near the band edge, it locally behaves as a semi-circle. The $1/N$ expansion at a fixed q at the temperatures $1 < \beta J < N$ can only resolve the local $\sqrt{E - E_0}$ behaviour near the band edge, but not the global behaviour. In the double scaling limit $N \rightarrow \infty$ and $q \rightarrow \infty$, but keep $\lambda = q^2/N$ fixed, the action can be mapped to a 2d Liouville CFT in the kinetic space with the central charge $c \sim N/q^2 = 1/\lambda$ which is solvable at all energy scales⁸⁶. The DOS was shown to be a Gaussian when $c \gg 1$, a semi-circle when $c \ll 1$, a more complicated form when $c \sim 1$ (see also the footnote [46] in Ref.²⁸). However, only in the triple scaling limit $\lambda \rightarrow 0$ (namely, the central charge $c \rightarrow \infty$) and the low energy limit $E - E_0 \rightarrow 0$, at a fixed $(E - E_0)/J\lambda = z$, it reduces to the 1d Schwarzian which is the low energy limit of the SYK model.

Appendix D: The edge (low and high energy) states versus the bulk (intermediate energy) states in $q = 2$ and $q = 4$ complex SYK

In this appendix, we aim to demonstrate the connections and differences between the edge and bulk states in the Fock space. They can be studied by studied by $1/N$ expansion or RG and RMT respectively. This appendix is heavily cited in Sec.VI.

1. $q = 2$ Complex SYK model.

The $q = 2$ complex SYK was written in Eq.15:

$$H_2 = \sum_{i < j}^N K_{ij} c_i^\dagger c_j - \mu q_c \quad (D1)$$

Instead of using the grand-canonical ensemble, we choose canonical one with a fixed fermion number $Q_c = \sum_{i=1}^N c_i^\dagger c_i$. Then, the total Hilbert space can be decomposed into N blocks as $2^N = \sum_{q=0}^N C_N^q$.

For $Q_c = 1$, it is nothing but the single-particle sector with the dimension $C_N^1 = N$. Under the PH transformation P , it is mapped to its particle-hole conjugate sector $C_N^{N-1} = N$ which is nothing but the single-hole

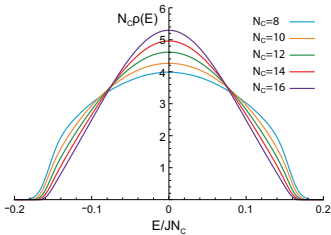


FIG. 12: The normalized many body DOS $\rho(E)$ for the half-filling sector of complex SYK model with $N_c = 8, 10, 12, 14, 16$. The numbers of samples are 50000 ($N_c = 8$), 10000 ($N_c = 10$), 2000 ($N_c = 12$), 400 ($N_c = 14$), 10 ($N_c = 16$).

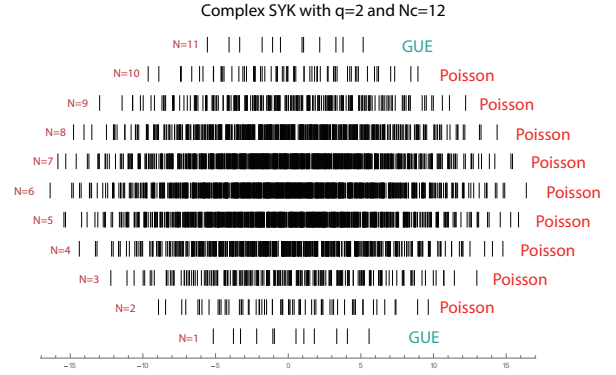


FIG. 13: The edge and bulk energy levels of $q = 2$ complex SYK at $N_c = 12$. The energy levels are labeled by conserved quantity (the number of fermion Q_c). Only the $Q_c = 1, 11$ sectors satisfy GUE, the others are Poisson. Note: $Q_c = 0$ and $Q_c = 12$ are two trivial sectors. The many body DOS at the half-filling is given in Fig.11b.

sector. Surprisingly and interestingly, only the single-particle and the single-hole sector are chaotic in the GUE, all the other multi-particle sectors $q \geq 2$ are integrable in the Poissonian (Fig.13).

As shown in Sec.III, $\{P, H_2\} = 0$, P also maps Q_c to $N_c - Q_c$. For N_c even, at the half-filling $Q_c = N_c/2$, so H_2 has a mirror symmetry for any realization of K_{ij} with respect to $E = 0$. This is indeed the case for $N_c = 12, Q_c = 6$ in Fig.13. However, the exact mirror symmetry is absent away from the half-filling. But as argued below Eq.D3, there is still an approximate mirror symmetry even away from the half-filling. Let us focus at the half-filling sector in the following.

As shown in Sec.V, the low energy spacing $\sim 1/N$ which stands for the low energy quasi-particle excitations, due to the exact mirror symmetry, the high energy spacing is also $\sim 1/N$ which stands for the high energy quasi-particle excitations. The bulk energy spacing is much smaller $\sim 1/C_N^{N/2} \sim \sqrt{N}2^{-N}$ at a large N . The KAM theorem is determined by the bulk energy spacing. All the bulk energy levels are described by the RMT in the Poisson statistics. The bulk energy level statistics is quite in-sensitive to the edge (low or high energy) levels will not affect the bulk Poisson statistics.

2. $q = 4$ Complex SYK model.

The $q = 4$ complex SYK was also written in Eq.15:

$$H_4 = \sum_{i < j, k < l}^N J_{ij;kl} c_i^\dagger c_j^\dagger c_k c_l - \mu q_c \quad (D2)$$

As shown in Sec.III, $[P, H_4] = 0$, so in contrast to H_2 , H_4 does not have a mirror symmetry for any given random realization of $J_{ij;kl}$. However, it still have an approximate mirror symmetry for any given realization

of J due to the following argument similar to Eq.18:

$$-H_4 = - \sum_{i < j, k < l}^N J_{ij;kl} c_i^\dagger c_j^\dagger c_k c_l = \sum_{i < j, k < l}^N J'_{ij;kl} c_i^\dagger c_j^\dagger c_k c_l \quad (\text{D3})$$

where $J'_{ij;kl} = -J_{ij;kl}$. Note that we are still confining to the $Q_c = \sum_{i=1}^N c_i^\dagger c_i$ sector. Obviously, J' and J satisfy the same distribution. At a large enough N_c , it is self-averaging, so there is still an approximate mirror symmetry at any filling for a given random realization of $J_{ij;kl}$.

This is indeed the case shown in Fig.14. As shown in Sec.VI, the low energy spacing $\sim e^{-s_0 N}$, due to the approximate mirror symmetry, the high energy spacing is also $\sim e^{-s_0 N}$. The bulk energy spacing is much smaller $\sim 1/C_N^{N/2} \sim \sqrt{N} 2^{-N}$. The KAM theorem is determined by the bulk energy spacing. All the bulk energy levels are described by the RMT in the GOE. The bulk energy level statistics is quite in-sensitive to the edge energy levels. Namely, incorporating or throwing away these edge

(low or high energy) levels will not affect the bulk GOE statistics.

It remains interesting to examine how the edge and bulk states evolve from the $q = 2$ side in Fig.13 to that in the $q = 4$ side in Fig.14 in the Type-I and Type-II hybrid complex SYK models.

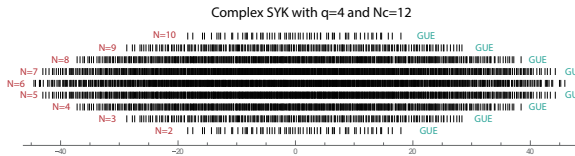


FIG. 14: The edge and bulk energy levels of $q = 4$ complex SYK and $N_c = 12$. The energy levels are labeled by conserved quantity, number of fermion Q_c . Only the $Q_c = 6$ sectors satisfy GOE, others are GUE. Note: For $Q_c = 1, N_c - 1$ stand for a single particle or hole, it is an exact zero modes with the degeneracy N_c . $Q_c = 0, 12$ are two trivial sectors. The many body DOS at the half-filling is given in Fig.12.

- ¹ A. I. Larkin and Y. N. Ovchinnikov, *Quasi-classical method in the theory of superconductivity*, Sov. Phys. JETP **28**, 1200 (1969).
- ² S. H. Shenker and D. Stanford, *Black holes and the butterfly effect*, J. High Energy Phys. 03 (2014) 067.
- ³ J. Maldacena, S. H. Shenker, and D. Stanford, *A bound on chaos*, J. High Energy Phys. 08 (2016) 106.
- ⁴ S. Sachdev and J. Ye, *Gapless spin liquid ground state in a random quantum Heisenberg magnet*, Phys. Rev. Lett. **70**, 3339 (1993).
- ⁵ A. Georges, O. Parcollet, and S. Sachdev, *Quantum fluctuations of a nearly critical Heisenberg spin glass*, Phys. Rev. B **63**, 134406 (2001).
- ⁶ A. Y. Kitaev, *A simple model of quantum holography*, talks at KITP, April 7, 2015 [http://online.kitp.ucsb.edu/online/entangled15/kitaev/], and May 27, 2015 [http://online.kitp.ucsb.edu/online/entangled15/kitaev/].
- ⁷ S. Sachdev, *Bekenstein-Hawking Entropy and Strange Metals*, Phys. Rev. X **5**, 041025 (2015).
- ⁸ J. Polchinski and V. Rosenhaus, *The Spectrum in the Sachdev-Ye-Kitaev Model*, J. High Energy Phys. 04 (2016) 001.
- ⁹ J. Maldacena and D. Stanford, *Remarks on the Sachdev-Ye-Kitaev model*, Phys. Rev. D **94**, 106002 (2016).
- ¹⁰ W. Fu and S. Sachdev, *Numerical study of fermion and boson models with infinite-range random interactions*, Phys. Rev. B **94**, 035135 (2016).
- ¹¹ D. J. Gross and V. Rosenhaus, *A Generalization of Sachdev-Ye-Kitaev*, J. High Energy Phys. 02 (2017) 093.
- ¹² D. Bagrets, A. Altland, and A. Kamenev, *Sachdev-Ye-Kitaev model as Liouville quantum mechanics*, Nucl. Phys. B **911**, 191 (2016).
- ¹³ D. Bagrets, A. Altland, and A. Kamenev, *Power-law out of time order correlation functions in the SYK model*, Nucl. Phys. B **921**, 727 (2017).
- ¹⁴ T. G. Mertens, G. J. Turiaci, H. L. Verlinde, *Solving the Schwarzian via the Conformal Bootstrap*, J. High Energy Phys. 08 (2017) 136.
- ¹⁵ D. Stanford, E. Witten, *Fermionic Localization of the Schwarzian Theory*, J. High Energy Phys. 10 (2017) 008.
- ¹⁶ J. Maldacena, D. Stanford, and Z. Yang, *Conformal symmetry and its breaking in two dimensional Nearly Anti-de-Sitter space*, Prog. Theor. Exp. Phys. 12 (2016) 12C104.
- ¹⁷ C. V. Johnson, *Jackiw-Teitelboim supergravity, minimal strings, and matrix models*, Phys. Rev. D **103**, 046012 (2021).
- ¹⁸ C. V. Johnson, *Explorations of nonperturbative Jackiw-Teitelboim gravity and supergravity*, Phys. Rev. D **103**, 046013 (2021).
- ¹⁹ A. Banerjee, A. Kundu, and R. R. Poojary, *Rotating black holes in AdS spacetime, extremality, and chaos*, Phys. Rev. D **102**, 106013 (2020).
- ²⁰ A. M. L. P. de Almeida, *Random Matrices and the Statistical Theory of Energy Levels*, Chapter 16, (Academic Press, 1967).
- ²¹ C. E. Porter, *Further remarks on energy level spacings*, Nuclear Physics **40**, 167 (1963),
- ²² P. B. Kahn and C. E. Porter, *Statistical fluctuations of energy levels: The unitary ensemble*, Nuclear Physics **48**, 385 (1963).
- ²³ Y.-Z. You, A. W. W. Ludwig, and C. Xu, *Sachdev-Ye-Kitaev Model and Thermalization on the Boundary of Many-Body Localized Fermionic Symmetry Protected Topological States*, Phys. Rev. B **95**, 115150 (2017).
- ²⁴ A. M. Garca-Garca and J. J.M. Verbaarschot, *Spectral and thermodynamic properties of the Sachdev-Ye-Kitaev model*, Phys. Rev. D **94**, 126010 (2016).
- ²⁵ J. S. Cotler, G. Gur-Ari, M. Hanada, J. Polchinski, P. Saad, S. H. Shenker, D. Stanford, A. Streicher, and M. Tezuka, *Black Holes and Random Matrices*, J. High Energy Phys. 05 (2017) 118 .
- ²⁶ T. Li, J. Liu, Y. Xin, Y. Zhou, *Supersymmetric SYK model and random matrix theory*, J. High Energy Phys. 06 (2017)

- 111 .
- ²⁷ T. Kanazawa, T. Wettig, *Complete random matrix classification of SYK models with $\mathcal{N} = 0, 1$ and 2 supersymmetry*, J. High Energy Phys. 09 (2017) 050 .
- ²⁸ F. Sun and J. Ye, *Periodic Table of SYK and supersymmetric SYK*, Phys. Rev. Lett. **124**, 244101 (2020).
- ²⁹ A. Altland and M. R. Zirnbauer, *Nonstandard symmetry classes in mesoscopic normal-superconducting hybrid structures*, Phys. Rev. B **55**, 1142 (1997).
- ³⁰ R. Gurau, *The complete $1/N$ expansion of a SYK-like tensor model*, Nucl. Phys. B **01** (2017) 015 .
- ³¹ E. Witten, *An SYK-Like Model Without Disorder*, J. Phys. A **52**, 474002 (2019).
- ³² I. R. Klebanov, G. Tarnopolsky, *Uncolored Random Tensors, Melon Diagrams, and the SYK Models*, Phys. Rev. D **95**, 046004 (2017).
- ³³ T. Nishioka, *Entanglement entropy: holography and renormalization group*, Rev. Mod. Phys. **90**, 035007 (2018).
- ³⁴ X.-G. Wen, *Colloquium: Zoo of quantum-topological phases of matter*, Rev. Mod. Phys. **89**, 041004 (2017).
- ³⁵ X. Chen and A. W. W. Ludwig, *Universal spectral correlations in the chaotic wave function and the development of quantum chaos*, Phys. Rev. B **98**, 064309 (2018).
- ³⁶ V. J. Emery and S. Kivelson, *Mapping of the two-channel Kondo problem to a resonant-level model*, Phys. Rev. B **46**, 10812 (1992). In fact, the non-zero impurity entropy at $T = 0$ appears first in the two-channel Kondo model: $s_0 = \log \sqrt{2}$ is due to a decoupled Majorana fermion at the impurity side. It also leads to a non-Fermi liquid (or bad metal) behaviours (or absence of quasi-particles), which also happen here in SYK models.
- ³⁷ A. W. W. Ludwig and I. Affleck, *Exact conformal-field-theory results on the multi-channel Kondo effect: Asymptotic three-dimensional space- and time-dependent multi-point and many-particle Green's functions*, Nucl. Phys. B **428**, 545 (1994).
- ³⁸ J. M. Maldacena, A. W. W. Ludwig, *Majorana Fermions, Exact Mapping between Quantum Impurity Fixed Points with four bulk Fermion species, and Solution of the "Unitarity Puzzle"*, Nucl.Phys. B506, 565 (1997).
- ³⁹ J. Ye, *On Emery-Kivelson line and universality of Wilson ratio of spin anisotropic Kondo model*, Phys. Rev. Lett. **77**, 3224 (1996),
- ⁴⁰ J. Ye, *Abelian Bosonization approach to quantum impurity problems*, Phys. Rev. Lett. **79**, 1385 (1997).
- ⁴¹ A. Y. Kitaev, *Anyons in an exactly solved model and beyond*, Ann. Phys. **321**, 2 (2006).
- ⁴² F. Sun, J. Ye, and W.-M. Liu, *Quantum magnetism of spinor bosons in optical lattices with synthetic non-Abelian gauge fields*, Phys. Rev. A **92**, 043609 (2015).
- ⁴³ For a concise review, see J. M. Deutsch, *Eigenstate Thermalization Hypothesis*, Rep. Prog. Phys. **81**, 082001 (2018).
- ⁴⁴ J. R. Garrison and T. Grover, *Does a Single Eigenstate Encode the Full Hamiltonian?*, Phys. Rev. X **8**, 021026 (2018).
- ⁴⁵ I. Kourkoulou, J. Maldacena, *Pure states in the SYK model and nearly-AdS2 gravity*, arXiv:1707.02325
- ⁴⁶ Y. Y. Atas, E. Bogomolny, O. Giraud, and G. Roux, *Distribution of the ratio of consecutive level spacings in random matrix ensembles*. Phys. Rev. Lett. **110**, 084101 (2013).
- ⁴⁷ S. Ryu, A.P. Schnyder, A. Furusaki and A.W.W. Ludwig, *Topological insulators and superconductors: Ten-fold way and dimensional hierarchy*, New J. Phys. **12**, 065010 (2010).
- ⁴⁸ M. Z. Hasan and C. L. Kane, *Colloquium: Topological insulators*, Rev. Mod. Phys. **82**, 3045 (2010).
- ⁴⁹ X. L. Qi and S. C. Zhang, *Topological insulators and superconductors*, Rev. Mod. Phys. **83**, 1057 (2011).
- ⁵⁰ C.-K. Chiu, J.C.Y. Teo, A.P. Schnyder and S. Ryu, *Classification of topological quantum matter with symmetries*, Rev. Mod. Phys. **88**, 035005 (2016).
- ⁵¹ In fact, equivalently, one can also define the PH symmetry operator to be $R = P(-1)^{Q_c} = (-1)^{N_c}(-1)^{Q_c}P = K \prod_{i=1}^{N_c} (c_i^\dagger - c_i)$. It is easy to show $R^2 = (-1)^{[\frac{N_c}{2}] + N_c}$, $Rc_iR = (-1)^{N_c-1}\eta c_i^\dagger$, $Rc_i^\dagger R = (-1)^{N_c-1}\eta c_i$, $R\chi_iR = (-1)^{N_c-1}\eta\chi_i$ where $\eta = (-1)^{[\frac{N_c-1}{2}]}$. The total number of fermions $Q_c = \sum_i c_i^\dagger c_i$. It is not a conserved quantity, but the parity $(-1)^{Q_c}$ is in H_{M4} . Then $RQ_cR^{-1} = N_c - Q_c$ which justifies R as an anti-unitary PH transformation. Here R does not provide any new information than P , so is redundant. But they become important and in-dependent anti-unitary operators in the $\mathcal{N} = 1$ SUSY SYK²⁶⁻²⁸. For a unified and compact classification scheme on both SYK and $\mathcal{N} = 1$ SUSY SYK, see²⁸.
- ⁵² Here we choose even site χ_{2i} to be real, odd site χ_{2i-1} to be pure imaginary. Then as shown in our recent work²⁸, by choosing this way, when N is odd, one must use the extended scheme (namely adding a Majorana fermion at ∞ to enlarge the Hilbert space twice, also introduce one more conserved quantity: the parity). However, if one choose the other way around, namely, even site χ_{2i} to be pure imaginary, odd site χ_{2i-1} to be real, then when N is odd, one can use either the minimum scheme without adding a Majorana fermion at ∞ or the extended scheme.
- ⁵³ It seems that so far, Ref.²³ and this work are the only two papers which have discussed the classifications and presented EDs in the odd N case. But the two papers still use different anti-unitary operators to do the RMT classifications. For example, Ref.²³ constructed an anti-unitary Time-reversal operator in the many body Hilbert space, while we did not have such a kind of operator. It is still not known to the authors what are the relations between the two different sets of anti-unitary operators. For a unified minimum classification scheme, see Ref.²⁸.
- ⁵⁴ In fact, here we discuss a canonical ensemble instead of a grand canonical ensemble. So it has a fixed N instead of a fixed μ .
- ⁵⁵ In all the Figs.4-8, we get more noises on the $q = 2$ side than those on the $q = 4$ sides. This is because at a given N , there are only N^2 random numbers K_{ij} on the $q = 2$ side, while there are much more N^4 random numbers J_{ijkl} on the $q = 4$ side. Of course, all q -SYK are quite sparse in RMT sense. The $q = 2$ side is just more sparse than the $q = 4$ side.
- ⁵⁶ L. Fidkowski and A. Kitaev, *Topological phases of fermions in one dimension*, Phys. Rev. B **83**, 075103 (2011).
- ⁵⁷ To do the ED, one^{10,23} puts the q complex fermions on a chain with N sites $i = 1, 2, \dots, N$, then use the Jordan-Wigner transformation $c_i = \sigma_i^- \prod_{j<i} \sigma_j^z$, $c_i = \sigma_i^+ \prod_{j<i} \sigma_j^z$ (or equivalently $\chi_{2i} = \sigma_i^x \prod_{j<i} \sigma_j^z$, $\chi_{2i-1} = \sigma_i^y \prod_{j<i} \sigma_j^z$) to map the spinless complex (or Majorana) fermion model to a quantum spin model, then do the ED in the equivalent quantum spin model. In this work, we did our ED in 3 independent ways (1) in the above spin basis after making the Jordan-Wigner transformation. (2) in the Hilbert space of complex fermions. As discussed in Sec.III-A, for odd N ,

- we add a Majorana fermion at $N + 1 = \infty$. (3) using the Clifford algebra for both $N = 2k$ even and $N = 2k + 1$ odd case. We achieved the same ED results in all the three ways.
- ⁵⁸ To do the ED, following Ref.¹⁰, one puts the Q_b hard core bosons on a chain with N sites $i = 1, 2, \dots, N$. The hard core boson case is simpler than its fermionic counterpart, because one do not need to attach a Jordan-Wigner string of σ_z , namely, $b_i = \sigma_i^-$, $b_i^\dagger = \sigma_i^+$ to map the hard core boson model to a quantum spin model.
- ⁵⁹ It was known that the quantum ferromagnetic and anti-ferromagnetic Heisenberg model differs by only a sign. Despite they have dramatically different ground states and low energy excitations, using the same argument here, one can see they share the same ELS.
- ⁶⁰ This choice is important when doing ED at a finite size N . However, choosing the four site indices all different or not makes no difference in the $1/N$ expansion.
- ⁶¹ Z. Bi, C.-M. Jian, Y.-Z. You, K. A. Pawlak, C. Xu, *Instability of the non-Fermi liquid state of the Sachdev-Ye-Kitaev Model*, Phys. Rev. B **95**, 205105 (2017).
- ⁶² A. Auerbach, *Interacting electrons and quantum magnetism*, (Springer Science & Business Media, 1994).
- ⁶³ S. Sachdev, *Quantum Phase transitions*, (2nd edition, Cambridge University Press, 2011).
- ⁶⁴ J. Ye and C.L. Zhang, *Super-radiance, Photon condensation and its phase diffusion*, Phys. Rev. A **84**, 023840 (2011).
- ⁶⁵ Yu Yi-Xiang, J. Ye and W.-M. Liu, *Goldstone and Higgs modes of photons inside a cavity*, Scientific Reports **3**, 3476 (2013).
- ⁶⁶ Yu Yi-Xiang, J. Ye, W.M. Liu and C.L. Zhang, *Comments on “Controlling Discrete and Continuous Symmetries in Superradiant Phase Transitions with Circuit QED Systems”*, arXiv:1506.06382.
- ⁶⁷ Yu Yi-Xiang, J. Ye and C.L. Zhang, *Parity oscillations and photon correlation functions in the $Z_2/U(1)$ Dicke model at a finite number of atoms or qubits*, Phys. Rev. A **94**, 023830 (2016).
- ⁶⁸ Yu Yi-Xiang, J. Ye, W.-M. Liu and C. L. Zhang, *Chaotic to integrable transition and a quantum analog of Kolmogorov-Arnold-Moser theorem in anisotropic Dicke model*, unpublished.
- ⁶⁹ J. Ye, *Two indices Sachdev-Ye-Kitaev model*, arXiv:1809.0667, substantially revised version 2 to be put on arXiv soon.
- ⁷⁰ R. Feng, G. Tian, D. Wei, *Spectrum of SYK model*, arXiv:1801.10073. Peking Math J. 2 (2019), No. 1, 41-70. *Spectrum of SYK model II: Central limit theorem*, arXiv:1806.05714; *Spectrum of SYK model III: Large deviations and concentration of measures*, arXiv:1806.04701. Random Matrices Theory Appl. 9 (2020), No. 2, 2050001 24pp. 60B20 (60F10)
- ⁷¹ F. Sun *et. al.*, preprint in preparation.
- ⁷² A. Almheiri, *Holographic Quantum Error Correction and the Projected Black Hole Interior*, arXiv:1810.02055.
- ⁷³ A. M. Garca-Garca, B. Loureiro, A. Romero-Bermdez, and M. Tezuka, *Stability of chaos in a generalised Sachdev-Ye-Kitaev model*, Phys. Rev. Lett. **120**, 241603 (2018). Unfortunately, this paper confused CIT with the QPT. It even applied finite size scaling to the CIT. As demonstrated in Sec.V, CIT is dramatically different from the QPT, the finite size scaling applies to the latter only, NOT to the former.
- ⁷⁴ T. Nosaka, D. Rosa, and J. Yoon, *The Thouless time for mass-deformed SYK*, J. High Energy Phys. 09 (2018) 041.
- ⁷⁵ F. Sun, Yu Yi-Xiang, J. Ye and W.-M. Liu, *Classifications of quantum chaos in colored Sachdev-Ye-Kitaev models*, Phys. Rev. D **101**, 026009 (2020).
- ⁷⁶ E.P. Wigner, *On the statistical distribution of the widths and spacings of nuclear resonance levels* Proc. Camb. Phil. Soc., No. **47**, 790 (1951).
- ⁷⁷ F. Dyson, *Statistical Theory of the Energy Levels of Complex Systems. I* J. Math. Phys. (N.Y.) **3**, 140 (1962).
- ⁷⁸ K. Efetov, *Supersymmetry in Disorder and Chaos*, (Cambridge University Press, 1996).
- ⁷⁹ J. Ye, *Coulomb interaction at Superconductor to Mott-insulator transition*, Phys. Rev. B **58**, 9450 (1998).
- ⁸⁰ J. Ye and S. Sachdev, *The effects of Coulomb interaction on Quantum Hall critical points of systems in a periodic potential*, Phys. Rev. Lett. **80**, 5409 (1998).
- ⁸¹ J. Ye, *The effects of weak disorders and Coulomb interaction on Quantum Hall critical points*, Phys. Rev. B **60**, 8290 (1999).
- ⁸² E.V. Shuryak and J.J.M Verbaarschot, *Random matrix theory and spectral sum rules for the Dirac operator in QCD*, Nucl. Phys. A 560 (1993) 306.
- ⁸³ J.J.M. Verbaarschot, *Spectrum of the QCD Dirac operator and chiral random matrix theory*, Phys. Rev. Lett. **72**, 2531 (1994).
- ⁸⁴ Takuya Kanazawa, and Tilo Wettig, *Stressed Cooper pairing in QCD at high isospin density: effective Lagrangian and random matrix theory*, J. High Energy Phys. 1410 (2014) 55.
- ⁸⁵ L. Herviou, J. H. Bardarson, and N. Regnault, *Many-body localization in a fragmented Hilbert space*, Phys. Rev. B 103 134207 (2021).
- ⁸⁶ M. Berkooz, M. Isachenkov, V. Narovlansky, and G. Torrents, *Towards a full solution of the large N double-scaled SYK model*, J. High Energy Phys. 03 (2019) 079.
- ⁸⁷ Y. Gu, A. Kitaev, S. Sachdev, and G. Tarnopolsky, *Notes on the complex Sachdev-Ye-Kitaev model*, J. High Energy Phys. 02 (2020) 157.
- ⁸⁸ In the $U(1)$ Dicke model⁶⁵, at any finite N , the gapless Goldstone mode at $N = \infty$ was lifted to a pseudo-Goldstone one with a finite gap $\Delta \sim D/N$ where D is the diffusion constant subject to an oscillation due to the Berry phase. Then when adding a small CRW term $\beta = g'/g < \beta_{U(1)} \sim 1/N^2$ smaller than this gap opened by the finite size effect, then the pseudo-Goldstone mode remains robust. This is more similar to the $q = 2$ integrable side where the quasi-particle exists and has a gap $\sim 1/N$, but dramatically different than the $q = 4$ quantum chaotic side where the quasi-particle breaks down and has a much smaller gap $\sim e^{-s_0 N}$ and all the low energy levels are also strongly repelled.
- ⁸⁹ The edge states here mean the many body energy levels near the ground state, so they are ground state plus low energy excitations. The edge exponents in the RMT for the 7 classes with a mirror symmetry²⁸ mean the asymptotic behaviour of the lowest eigenvalue λ_1 near the origin $E = 0$ which, in the present case, is one of the bulk states. In some literatures, the former is called soft edge, the latter is hard edge.
- ⁹⁰ There should be an exact proof on this Gaussian distribution in the many body DOS, see⁷¹.
- ⁹¹ The two ways flow between the two CFT₁ fixed points in Fig.9b1 and 9b2 violates the Zamolodchikov’s c-theorem

on RG flow between two CFT_2 fixed points. See the conclusion section for more discussions.